Iran J Earth Sci., 2026; 18(2): 146-175

Iranian Journal of Earth Sciences (IJES)

https://doi.org/10.57647/j.ijes.2025.16851

Research Article

Satellite Data and Applying the DSAS Tool to Shoreline Change Assessment of the Mekong Delta

Bui Minh Quan[1], Ngo Thi Kim Chi[1]*, Bui Vinh Hau[1], Nguyen Dac Ve[2], Binbin Jiang[3,4]

[1]*Hanoi University of Mining and Geology, Vietnam*
[2]*Institute of Marine Environment and Resources (IMER), Vietnam Academy of Science and Technology (VAST), Haiphong, Vietnam*
[3]*School of Mechanical and Automotive Engineering, Zhejiang University science and Technology, Hangzhou, P.R.China*
[4]*Anji-zust research institute, Huzhou, P.R.China*

***Corresponding author:** ngothikimchi@humg.edu.vn

Article History:

Received:
7 September 2024

Revised:
26 October 2024

Accepted:
2 January 2025

Published Online:
25 May 2025

Published in Issue:
30 June 2026

Abstract

The Mekong Delta is the third-largest delta in the world, with a large population, a significant food production area in Vietnam and home to large-scale biodiversity, is seriously affected by erosion - accretion of the coast, land subsidence. Several dams have been built upstream of the delta (Manwan, Nuozhadu…), and large-scale commercial sand mining in the river and delta channels, along with subsidence caused by groundwater extraction, are the causes of sediment decline in the Mekong Delta. This affects the daily lives of more than 21 million people. Using high-resolution satellite imagery (Landsat) for the period 1989-2020, this paper assesses erosion-accretion rates at the Mekong estuary to Ca Mau cape. Extracting the shoreline using the Normalized Difference Vegetation Index used to measure vegetation change and the Digital Shoreline Analysis System used to analyze changes in the shoreline. The results show that the Mekong estuary is having an alternating process of erosion-accretion, the balance of erosion-accretion tends to imbalance with dominant accretion. The Mekong estuary area, including the Tieu, Dai, Ba Lai, Ham Luong, Co Chien, Cung Hau, Dinh An and Tran De mouths, experiences erosion and accretion ranging from 1.37 to 120.98 m/yr and 74.94 to 117.06 m/yr, respectively. From My Thanh mouth to Ca Mau Cape, with erosion ranging from 66.07 to 115.5 m/yr and accretion from 29.67 to 91.06 m/yr, respectively. Our research emphasizes the fragility of the Mekong Delta coastline and underscores the critical role of remote sensing imagery in effective shoreline management.

Keyword: Mekong Delta, erosion and accretion, Landsat, shoreline change

Cite this article: Minh Quan, B., Thi Kim Chi, N., Vinh Hau, B., Dac Ve, N. & Jiang., B., (2026). Iranian Journal of Earth Sciences, Satellite Data and Applying the DSAS Tool to Shoreline Change Assessment of The Mekong Delta, 18(2): 146-175. https://doi.org/10.57647/j.ijes.2025.16851

1. Introduction

As a place with flat terrain, fertile land, convenient transportation, etc., the population is concentrated mainly in large plains such as the delta of the Yangtze River, Ganges River, Nile River, Amazon River, etc. According to Syvitski's report, >37% of the world's population lives within 100 km of the coast, and about 44% of the population lives within 150 km of the coast. But recently,

coastal erosion has become a problem for most of the world's plains. The stability of the shoreline depends on the ratio between the sediment supply and the accommodation space generated by sea level rise and subsidence (Bera and Maiti, 2019). If the sediment supply exceeds the rate of relative sea level change, the delta will prograde; otherwise, it will retreat through shoreline erosion (Bera and Maiti, 2019).

The Mekong River is one of the world's largest rivers, with a basin of more than 900,000 km^2, and it is also the 12th longest river, with the world's 8th greatest water discharge and the 10th largest sediment (Meade, 1996; Li et al., 2017). The Mekong River (Fig. 1a) is in the mountainous area of the Tibet Plateau and flows through China, Myanmar, Laos, Thailand, Cambodia, and Vietnam into the East Sea (Bien Dong). Its annual water discharge is ~470×10^9 m^3, and the annual sediment flux was ~130-160 million tons (Mt) in the 1960s (Milliman and Syvitski, 1992; Arjmandzadeh et al. 2017) and 110 Mt in the 1990s (Milliman and Farnsworth, 2011). The Mekong River flows into Vietnam through two main distributaries: the Tien River (generally referred to as the Mekong River) in the north, accounting for nearly 58% of the total water volume of the Mekong River, and the Hau River (also known as the Bassac River) in the south, accounting for 42% of the Mekong River's discharge (Yazdi et al. 2016; Gugliotta et al., 2017; Ha et al., 2018) (Fig. 2). The river discharge of the Mekong is mostly controlled by the tropical Monsoon climate, which has distinct flood and dry seasons (Lu and Siew, 2006). Flood season (May to October) accounts for 85% of water discharge, and 15% occurs in the dry season (November to April) (Unverricht et al., 2013).

The river in Vietnam shapes the third-largest delta globally, spreading wide across the landscape (Coleman and Roberts 1989; Ta et al., 2001; Anthony et al., 2015). The average accretion rate of the entire delta in the past 7000 years was 30 m/yr (Liu et al., 2017). The Mekong Delta has transitioned from being "tide-dominated" to "tide-and-wave dominated" at a rate of 16 m/yr in the Mekong estuary and 26 m/yr in Ca Mau. (Ta et al., 2002; Li et al., 2017). The tide-dominated delta has a well-developed mangrove forest on the subaerial delta plain, cross-shore sediment dispersal, and tide-influenced sedimentary facies, whereas the tide-and-wave-dominated delta has a beach-ridge system on the subaerial delta plain, longshore sediment dispersal, and a steep delta-front topography (Ta et al., 2005). The estuary is considered to extend from the inner limit of tidal facies at its head to the outer limit of coastal facies at its mouth (Dalrymple et al., 1992). Based on the calculated salinity intrusion, the combination of channels is considered one (Bassac and Co Chien channels). The salinity intrusion is measured from the Bassac channel (a combination of Tran De and Dinh An) at approximately 50 km (Nguyen and Savenije, 2006). The salinity intrusion is measured from the Co Chien channel (a combination of Co Chien and Cung Hau) at approximately 40 km (Nguyen and Savenije, 2006). Given the similarity among the river channels, we can infer that the Ham Luong channel and the My Tho channel are 40–50 km from the mouths (Fig. 1b).

However, human activities are seriously altering the amount of sediment discharged by rivers (Syvitski et al., 2005), e.g., the construction of hydroelectric dams and illegal sand mining. Globally, about 53% of sediment load is currently trapped in reservoirs, with 30% in large reservoirs and 23% in small reservoirs (Vörösmarty et al., 2003). The Vietnam-Mekong Delta's annual sediment budget has decreased from 39 Mt/yr in 1993 to 28 Mt/yr in 2015. In 2015, the sediment budget of Vietnam's Mekong Delta was reduced by 83% as compared to the pre-dam (before 1992) sediment budget of 160 Mt/yr (Milliman and Syvitski, 1992; Binh et al., 2018). Since the mid-twentieth century, the evolution of the Mekong Delta has been increasingly influenced by human activities such as land subsidence owing to groundwater extraction, reduction of river fluxes due to damming and sand mining, and reduction of protective coastal zones (Marchesiello et al., 2019). The Mekong Delta's shoreline is now being retrograded, and several coastal provinces are suffering from major impacts of vegetation erosion, including saltwater intrusion and land subsidence (Anthony et al., 2015; Smajgl et al., 2015; Liu et al., 2017; Minderhoud et al., 2017). Between 2003 and 2012, dam sediment impoundment caused a 5% annual decline in suspended sediment concentrations of the delta (Loisel et al., 2014). Riverbed mining has also grown in popularity during the last decade, particularly in Cambodia and Vietnam (Bravard et al., 2013). In general, erosion and accretion occur alternately at the mouth of the Mekong River and along the southern shoreline of the estuary to Ca Mau Cape. Using high-resolution SPOT 5 satellite images from 2003 to 2012, Anthony et al., (2015) described the erosion and accretion across 600 km of the Mekong Delta in response to human activities. Whereas, Besset et al., (2015) proved that the Mekong Delta's erosion is mostly explained by high rates of shoreline retreat along the East Sea (Bien Dong) sector downdrift of the mouths. Besset et al., (2016) recently analyzed data from Landsat 1–5 MSS and Landsat 8 OLI images from 1973 to 2015 along the southern bank of the Mekong estuary (from My Thanh mouth to Ca Mau Cape). Phan et al., (2017) research was updated for the whole Mekong Delta, spanning from the Tieu mouth to the Kien Giang province for 43 years (from 1973 to 2015). Accretion and erosion alternately occur along the delta coast (from the Soai Rap mouth to the Cai Lon mouth), and

the total shoreline change rate has significantly decreased over the past four decades (Li et al., 2017). The climate of the Mekong Delta is demonstrated by the Southwest (SW) Monsoon from the sea; it is wet and rainy, and May to October is the rainy season (Unverricht et al., 2013). November to April of the following year, it is affected by the Northeast (NE) Monsoon coming from the mainland, which is arid with little rain; November to April is the dry season (Commission Mekong River, 2005; Unverricht et al., 2013) (Fig. 3a). Thunderstorms have great intensity, a relatively short duration, and a small influence range, and they are very frequent during the rainy season. Rainfall has a relatively long time and a very large range, most often in August and September, which can lead to severe flooding. The Mekong Delta is exposed to low-to-moderate energy waves from the southwest during the SW Monsoon season that generate weak longshore currents towards the northeast, a situation that favors the mud storage in the river mouth sector. The NE Monsoon season is characterized by higher waves responsible for the active alongshore sediment transport westwards from the mouths (Anthony et al., 2015).

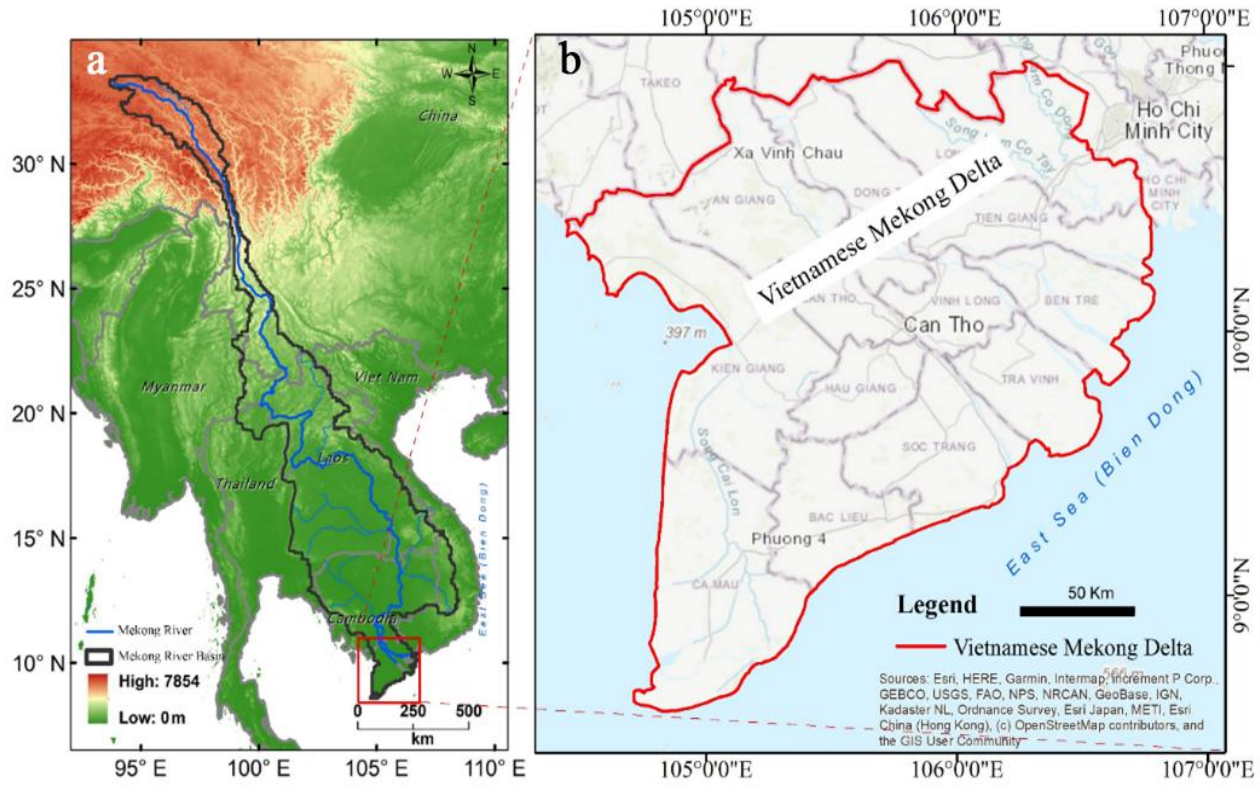

Figure 1. a) The Mekong River Basin and its delta (adapted from Li et al., 2023). b) Vietnamese Mekong Delta

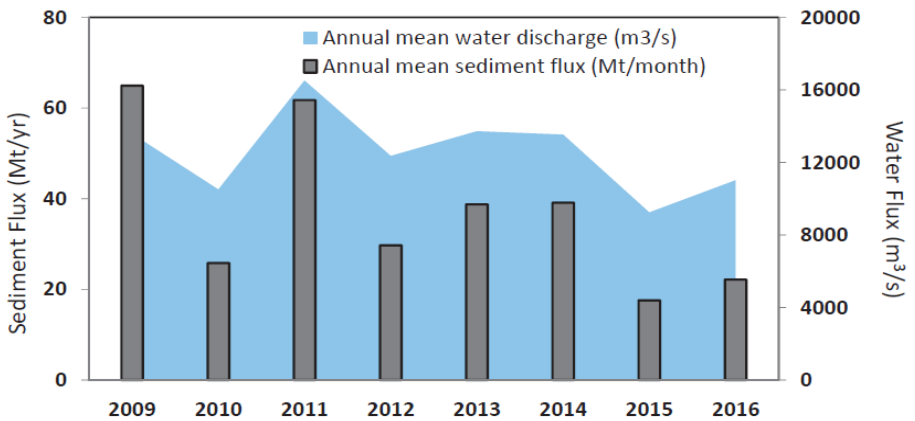

Figure 2. Evolution of annual mean water discharge (m^3/s) and sediment flux (Mt/yr) of the Mekong River from 2009-2016 (from Ha et al., 2018)

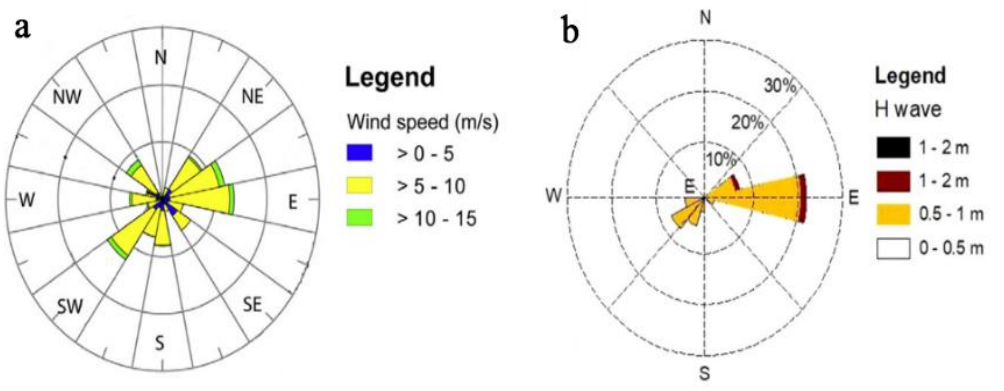

Figure 3. a) The wind rose for the East bank of the Mekong Delta in the East Sea(Bien Dong) (Unverricht et al., 2014). b) Wave rose for the East bank of the Mekong Delta (East Sea (Bien Dong) - adapted from these manuscripts (Anthony et al., 2015; Khoi et al., 2020)

The wave climate differs significantly between the annual seasons and the Mekong Delta subareas (Unverricht et al., 2014). In the river mouth region, significant wave heights of more than 1 m can occur at the shoreline for the whole year (Tamura et al., 2010; Unverricht et al., 2014). In Vinh Tan (close to Bac Lieu), southwest of the Bassac distributary (Fig. 3b), significant wave heights of 0.2–0.25 m and up to 0.55 m, respectively, were measured 300 m from the shoreline (Unverricht et al., 2014). On the east bank of the Mekong Delta, the tides are semidiurnal, with two high tides and two low tides per day (with tidal ranges of 2.5–3.8 m).

In general, the study area is a densely populated place, urban area, seaport, industrial center, economic activity, with important significance in both socio-economic and national security and defense. On the other hand, dynamic changes in the shoreline can cause geological disasters, greatly affecting the lives of local people.

Existing studies only cover a limited period, frequency, or spatial extent, which is insufficient to uncover precise and holistic shoreline alterations. The study period of a long period (15 years to over 20 years per phase) (Phan et al., 2017) or a short study period (2003–2012) (Anthony et al., 2015). The novelty of this study lies in its integration of long-term satellite data and cutting-edge geospatial techniques, enabling the more precise detection of subtle but significant changes in coastal processes. Furthermore, the research will contribute to a more robust understanding of how factors such as upstream damming, land subsidence, and sea-level rise are impacting the delta. This will support the development of forward-looking coastal management strategies, making it a valuable resource for policymakers and environmental planners aiming to mitigate disaster risks and enhance the resilience of coastal systems. The main objective of the study is to utilize advanced techniques such as Remote Sensing (RS) and Geographic Information Systems (GIS) to describe the extent of coastal changes and analyze shifts in coastal dynamics, including erosion and accretion, over a period of time. Additionally, it aims to develop effective coastal management plans and mitigate the impact of natural and human-induced factors on the coastline.

Effective coastal management is increasingly essential in the face of rising sea levels, intensified storm activity, and human-induced changes such as dam construction and land use modifications. This research contributes to the development of strategic plans to safeguard coastal communities and ecosystems by informing decision-makers on erosion control measures and sustainable development. Moreover, by analyzing sediment transport dynamics, the study sheds light on the intricate balance between riverine sediment discharge and coastal processes, which is key to maintaining delta stability and mitigating risks associated with land subsidence and flooding.

2. Materials and methods

2.1. Study area

The research area has relatively low and flat terrain, with an average slope of 1 cm/km, and the average height above sea level is less than 2 meters. This area primarily consists of Quaternary sediments and sedimentary rocks. The Cenozoic granitoid rocks are scattered as small bodies in the western study area (An Giang province) (Do, 2016). The Mekong River flows into Vietnam through two main tributaries: The Tien River (generally referred to as the Mekong River) in the north, which accounts for nearly 58% of the total water volume of the Mekong River, and the Hau River (also known as the Bassac River) in the south, which accounts for 42% of the Mekong River's discharge (Gugliotta et al., 2017; Ha et al., 2018).

The study area is located in the eastern portion of the Mekong Delta, extending about 530 km from Tieu estuary

(Tien Giang province) to Ca Mau cape (Ca Mau province), between 8°33' N to 10°25'N and 104°48'E to 106°48'E (Fig. 1b). The climate in the Mekong Delta is characterized by tropical monsoons, with a distinct wet season and dry season (Lu and Siew, 2006). The average annual rainfall of the Mekong Basin is 1512 mm (1950–2016) (Pawar et al., 2023). The discharge is at its highest in the wet season, from August through September, when 85% of the water discharge occurs, and at its lowest in the dry season, from April to May, when 15% of the water discharge occurs (Kummu et al., 2008; Unverricht et al., 2013). The tides are semidiurnal, with two high tides and two low tides per day. According to the General Statistics Office in 2019, the Mekong Delta has a total population of more than 17 million people, accounting for 18% of the population of Vietnam. Rice alone accounts for 47% of the area and 56% of the country's rice production; rice exports from the whole region account for 90% of production. Seafood accounts for 70% of the area, 40% of production, and 60% of the country's exports. These important advantages are increasingly threatened by some rapid development drivers, notably proposed large-capacity hydroelectric dams, riverbed mining, river sediment supply, and the future stability of the Mekong Delta (Anthony et al., 2015).

2.2. Data sources

Landsat, a joint program of the United States Geological Survey (USGS) and the National Aeronautics and Space Administration (NASA), has been observing the Earth continuously from 1972 through the present day. Landsat 5 carried the Multispectral Scanner (MSS) and the Thematic Mapper (TM) sensors. Landsat 5 was operational from 1984 to 2013, providing a long historical record of Earth observation data. This makes it valuable for studying long-term changes in the environment. Landsat 8 provides continuity with the more than 40-year-long Landsat land imaging data set. Landsat-8, launched in 2013, is equipped with the Operational Land Imager (OLI) and the Thermal Infrared Sensor (TIRS). These sensors offer improved radiometric resolution, more spectral bands (11 in total), and enhanced capabilities for detecting finer details and subtle changes in the landscape. Landsat 8 provides 12-bit data, allowing for greater differentiation between land cover types and more detailed analysis of subtle variations in reflectance values. In addition to widespread routine use for land use planning and monitoring on regional to local scales, support of disaster response and evaluations, and water use monitoring, Landsat 8 measurements directly serve NASA research in the focus areas of climate, carbon cycle, ecosystems, water cycle, biogeochemistry, and Earth surface/interior (https://www.usgs.gov/). Satellite images of the Mekong Delta from 1989 to 2020 were used to analyze morphological changes in the Mekong Delta. The Landsat 5, 8 images (30 m spatial resolution) were downloaded free from the website of the United States Geological Survey (http://earthexplorer.usgs.gov/).

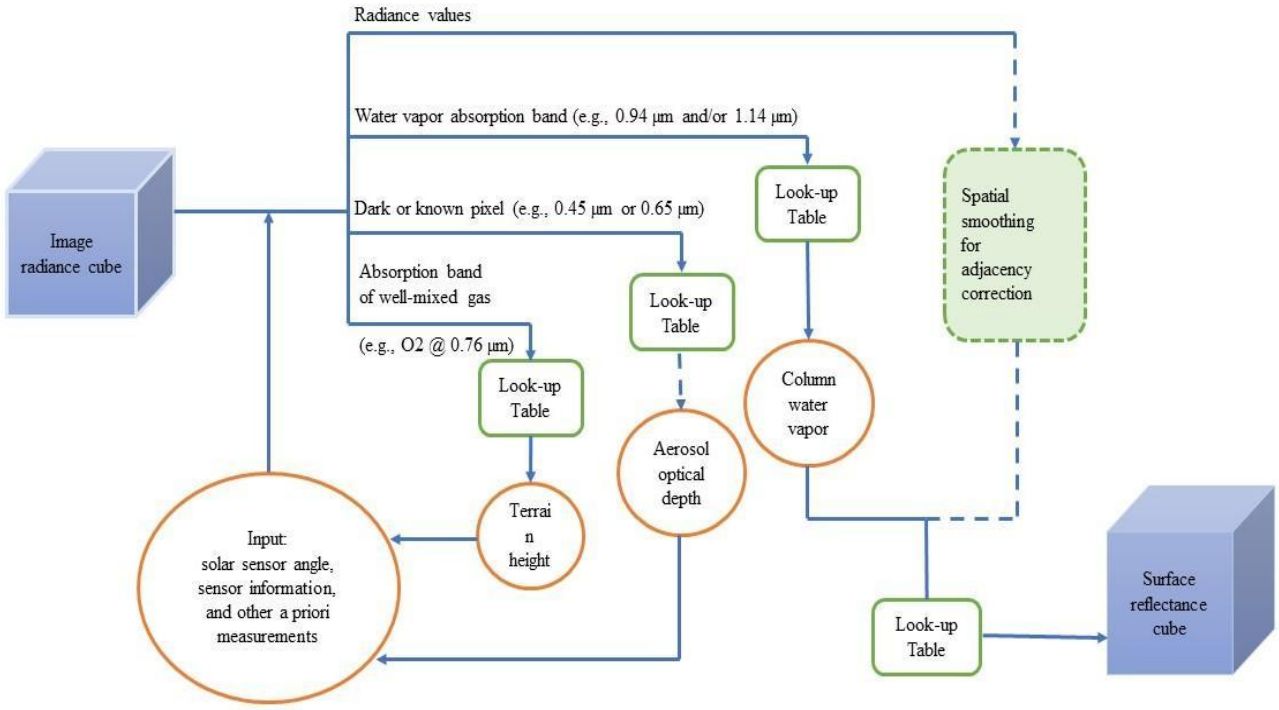

Figure 4. The FLAASH schematic flow defines the basic steps to convert the sensor-measured radiance to surface reflectance (Griffin et al., 2003)

The 30-meter spatial resolution of Landsat imagery provides a balance between spatial coverage and data availability, making it useful for long-term monitoring of the Mekong Delta. This resolution is effective for monitoring shoreline retreat and sediment discharge in the delta.

Landsat was likely chosen because it provides the optimal mix of historical continuity, global coverage, cost-effectiveness, and moderate spatial resolution for analyzing the Mekong Delta's geomorphological changes.

2.3. The digital shoreline analysis system (DSAS)

Images have been atmospherically corrected using FLAASH on the ENVI 5.3 application improving the quality and reliability of remote sensing data (Fig. 4). Assessing the spatial dynamics of coasts requires consideration of both historical history and morphodynamics. DSAS software (version 4.3), an Esri ArcGIS (10.1) desktop add-in, allows users to calculate the rate of statistical change from various historical shoreline positions. Data after being calculated in ArcGIS, will be exported to Excel for processing and statistics. It is one of the most broadly utilized techniques for the analysis of such studies in the world. It provides an automated method for establishing measurement locations, performs rate calculations, provides the statistical data necessary to assess the robustness of the rates, and includes a beta model of shoreline forecasting with the option to generate 10- and/or 20-year shoreline horizons and uncertainty bands (Thieler et al., 2009). The DSAS operational workflow includes 7 steps (see workflow, Fig. 5):

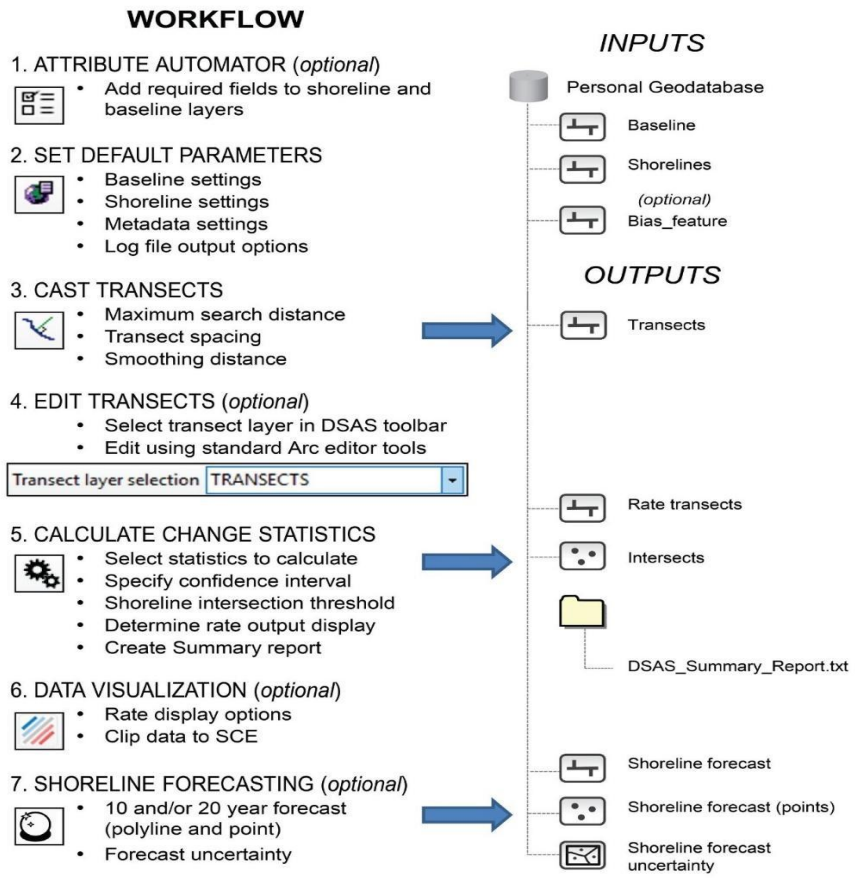

Figure 5. The Digital Shoreline Analysis System (DSAS) workflow with stepsnecessary to establish transects (Thieler et al., 2009)

1. ***Attribute automator***: add required and optional fields to one or more selected shoreline and baseline feature classes within a geodatabase.
2. ***Set default parameters***: baseline, shoreline, metadata, and log file output options.
3. ***Cast transects***: generates a new (or overwrites an existing) transect feature class by using the user-specified settings in Default Parameters.
4. ***Edit transects***: modify the baseline and directly edit individual transects.
5. ***Calculate change statistics***: select a list of change-rate statistics to be calculated.
6. ***Data visualization:*** includes options to alter the

change-rate color options or generate a copy of the specified transect file that is clipped to the shoreline change envelope (VCE).

7. ***Shoreline forecasting:*** combines observed shoreline positions and model-derived shoreline positions, to predict future shoreline positions with an associated uncertainty.

This program creates transects perpendicular to the shoreline at a user-specified distance. In order to calculate the morphological changes of the coast during the period 1989–2020. The rate of change statistics is then computed using the transect intersection position of the shoreline along a baseline, including:

Net Shoreline Movement (NSM) reports the distance (not a rate) between the oldest and youngest shoreline for each transect; this represents the total distance between the oldest and youngest shoreline. It is expressed as:

$$NSM = SL_0 - SL_1$$

Where NSM is a net shoreline movement in the position of shoreline (m); SL_0 is the distance between baseline and shoreline (m) in the considered old date at a transect; and SL_1 is the distance between baseline and shoreline (m) in the latest date at the same position or transect.

The End Point Rate (EPR) is calculated by dividing the distance of shoreline movement by the time elapsed between the oldest and the most recent shoreline. The major advantages of the EPR are the ease of computation and the minimal requirement of only two shoreline dates. The EPR is estimated at:

$$EPR = \frac{(SL_0 - SL_1)}{t}$$

Where t is the time elapsed between the two shoreline positions.

Linear Regression Rate (LRR), a linear regression rate of change statistic, can be determined by fitting a least-squares regression line to all shoreline points for a particular transect. The regression line is placed so that the sum of the squared residuals (determined by squaring the offset distance of each data point from the regression line and adding the squared residuals together) is minimized. The linear regression rate is the slope of the line (Thieler et al., 2009).

2.4. Analysis of mekong shoreline changes

Several methods and techniques have been developed to account for the morphological changes along the coast. But delineating the vegetation of any plain is a difficult process because of the presence of various natural agents such as sea dikes, areas of swamps, and intertidal flats. Most of the Mekong Delta is lined with mangroves (Gebhardt et al., 2012). Mangroves are considered to be the best geological indicator in global shoreline change research (Souza Filho et al., 2006). Mangroves have certain heights, which means that the tidal cycle has little influence on the shoreline position (Phan et al., 2015). Therefore, the mangrove boundary was used as a shoreline indicator to detect the coastal change in this study. Moreover, using satellite imagery makes it easy to distinguish the boundary of mangrove vegetation using the Normalized Difference Vegetation Index (NDVI). The spatial-temporal variations in the evolution and retreat in the Mekong Delta can be determined based on the changes in the position of the shoreline.

According to Fletcher et al., (2012), five sources of uncertainty affect historical shoreline position accuracies and final change rates of shorelines derived from aerial photographs: seasons (waves), tides, digitization, image pixels, and rectification. In this study, we used shoreline from Landsat images for what. Mangroves with 8–12 m heights are dominant on the Mekong Delta coast (Tong et al., 2004; Gebhardt et al., 2012). The tidal regime is semi-diurnal, with a tidal range of approximately 2 m to 4 m along the East Sea (Bien Dong) coast. The mean wave height is 0.9 m (Ta et al., 2005). So the water-level changes induced by waves or tides would have relatively little effect on the shoreline position (Bao, 2011; Phan et al., 2015).

The NDVI developed by quantifies vegetation by measuring the difference between near-infrared (which vegetation strongly reflects) and red light (which vegetation absorbs) (Rouse et al., 1973). The NDVI is calculated for each image (1989, 1998, 2008, and 2020) after performing atmospheric correction image preprocessing, and the NDVI is calculated by equation:

$$NDVI = \frac{(\rho NIR - \rho RED)}{(\rho NIR + \rho RED)} \quad (1)$$

Where ρRED represents the red band reflectance from satellite (band 3 for Landsat 5 and band 4 for Landsat 8), and band ρNIR is the near-infrared band (band 4 for Landsat 5 and band 5 for Landsat 8).

NDVI always ranges from -1 to +1. When NDVI has a negative value, it represents water. When NDVI is positive, it can indicate urbanized areas, and when it approaches +1, it represents dense green leaves.

2.5. Uncertainty analysis

The positive and negative values obtained from the DSAS in the result indicate accretion and erosion, respectively. Analysis performance using DSAS will have errors based on the factors of uncertainty. The accuracy of such an analysis on the shoreline position and change rate in the

shoreline is influenced by several uncertainties, such as image resolution, image registration, digitization error, position of tidal level, and elevation-related issues (Jayson-Quashigah et al., 2013; Vu et al., 2020). Therefore, the shoreline positional error (E_a) for individual transects was calculated using:

$$E_a = \pm\sqrt{E_s^2 + E_w^2 + E_d^2 + E_r^2 + E_p^2}$$

where E indicates different types of Error such as E_s is the seasonal, E_w is the tidal level, and E_d is the digitization E_r is the rectification and E_p is the pixel error, respectively. This approach considers that component errors are distributed normally (Dar and Dar, 2009). These errors were used as weights in the total uncertainties of the change in shoreline calculations. The values were averaged for the period (year) to provide the error (E_u) estimation for the shoreline change rate at any given transect and is expressed as:

$$E_u = \frac{\pm\sqrt{U_{t1}^2 + U_{t2}^2 + U_{t3}^2 + U_{t4}^2 + \cdots + U_{tn}^2}}{T}$$

where t_1, t_2, and t_n are the total shoreline position error for the various years and, in this study, its T is a 31-year period of analysis.

2.6. Field survey

A field survey is a method of collecting the data of a specific area or location by conducting an on-site investigation. We surveyed the estuary of the Mekong Delta in July 2022 (flood season) and February 2023 (dry season). The survey spans from the mouth of Dai to Bac Lieu province along the coast of the Mekong Delta. During the survey, a handheld GPS was used to determine the exact location of the survey point (Garmin GPS 73). The purpose of the survey was to verify the results of remote sensing image processing. At the same time, survey erosion and accretion in areas that are frequently retreated in the Mekong Delta (Fig. 6).

3. Results

Remote sensing data is increasingly used to monitor coastal features. Vegetation has been defined based on the wet-dry boundary or the vegetation-bare-flat boundary on satellite images. However, these two boundaries are difficult to assign to some specific tidal elevations because of irregular vegetation fronts and changing water levels when each satellite image is shot at a different tidal stage (Fan et al., 2019). In this study, we propose that application of shoreline to study the evolution of coastal areas in the Mekong Delta.

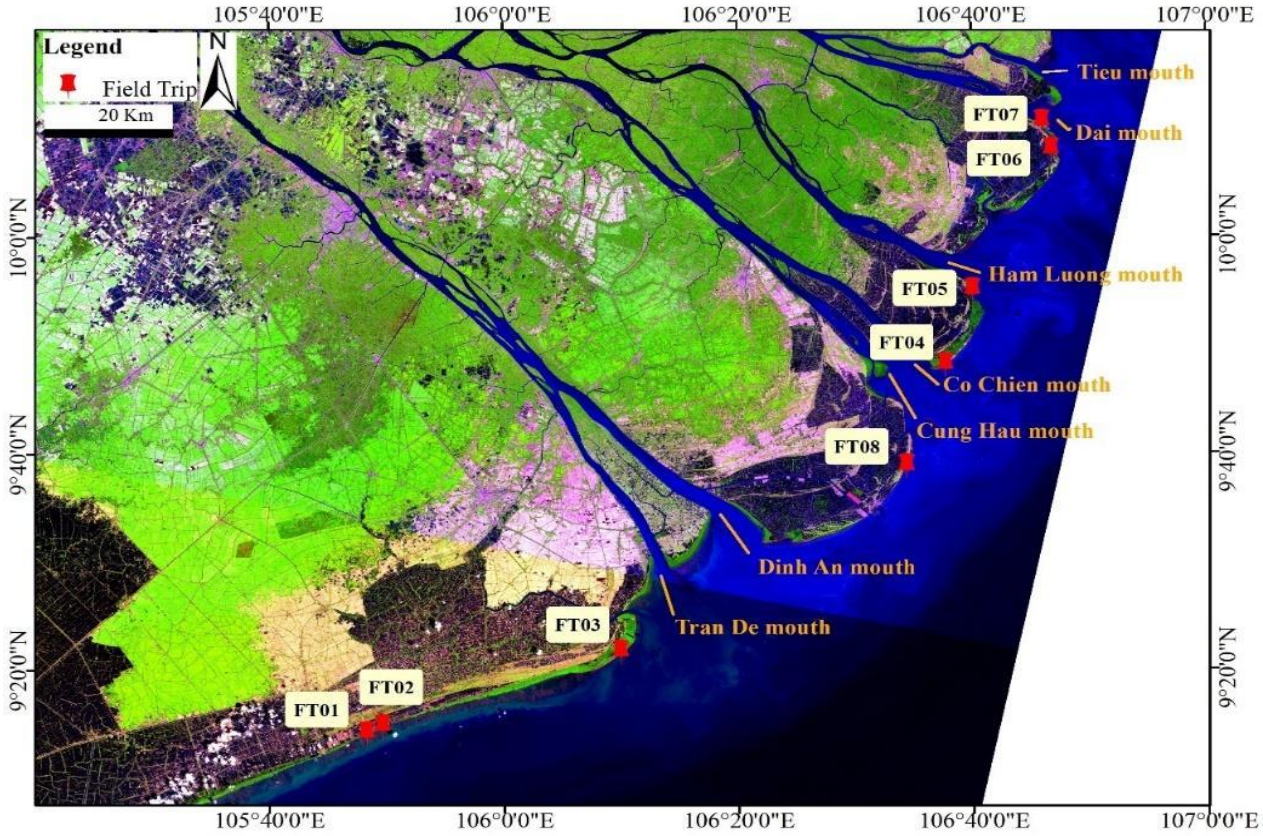

Figure 6. Field Trip (FT01-08) from Bac Lieu province to Dai mouth (Jul/2022 and Feb/2023)

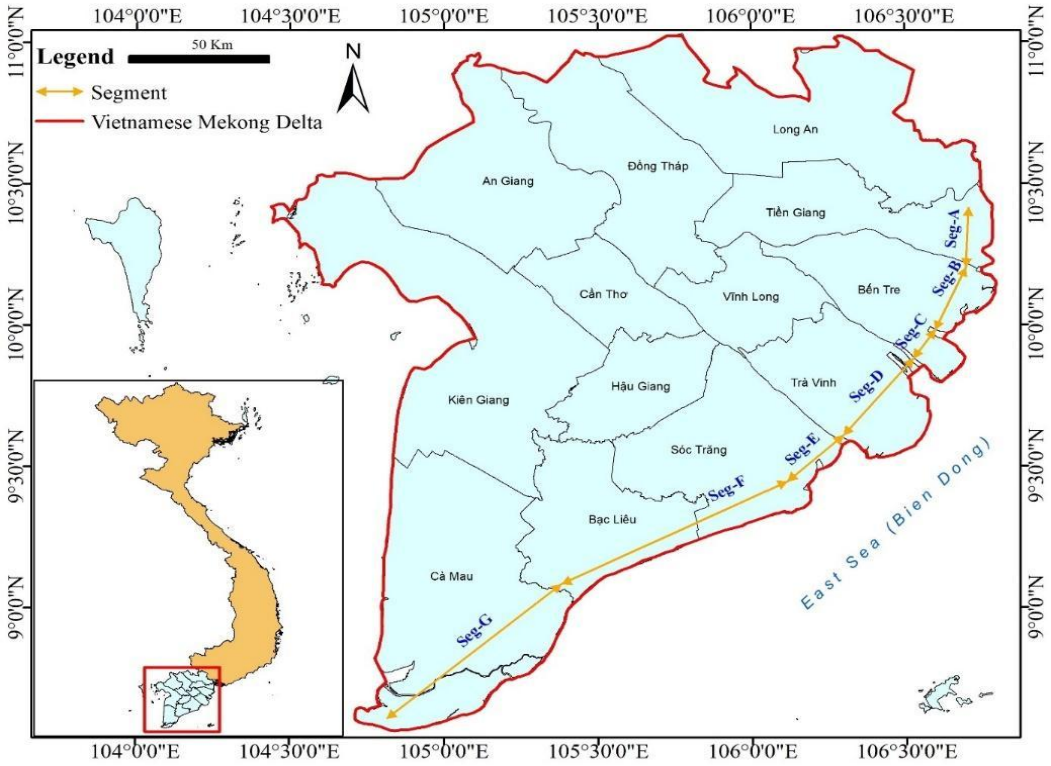

Figure 7. The location of 7 segments in this study

Table 1. DSAS transect description in the study area

Parameters \ Segment	A	B	C	D	E	F	G
Number of transects	1169	1590	1040	2380	917	3551	3186
Transect spacing (m)	30	30	30	30	30	30	30
Average baseline distance from the shoreline (m)	300	300	300	300	300	300	300

NDVI quantifies vegetation by measuring the difference between near-infrared (which vegetation strongly reflects) and red light (which vegetation absorbs). NDVI is a standardized way to measure healthy vegetation.The study area is divided into 7 segments: segment A (Tieu mouth to Dai mouth), segment B (Ba Lai), segment C (Ham Luong mouth), segment D (Co Chien mouth to Cung Hau mouth), segment E (Dinh An mouth to Tran De mouth), segment F (from My Thanh mouth to Ganh Hao mouth), and segment G (from Ganh Hao mouth to Ca Mau Cape) (Fig. 7).

The extracted shoreline from 1989–2020 (1989, 1998, 2008, 2020) was imported and merged into ArcGIS 10.1 software. DSAS uses a measurement baseline method to calculate rate of change statistics for a time series of shoreline. The baseline serves as the starting point for all transects cast by the DSAS application. The baseline was drawn at about a 3 km distance seaward, parallel to the shoreline orientation. The transect, each 3 km in length (3 km is an estimate of the distance from the baseline that can cross the shorelines of the years during the study period; outside this range, DSAS will ignore), at an equal spacing of 30 m along the baseline, was generated through DSAS software. A total of 13833 transects were cast at a 300-m interval along the baseline (Table 1).

3.1. Morphological change rates for a long period

The shoreline changes over the period 1989–2020 (31 years) were measured using the Linear Regression Rate (LRR) method. This method calculates the rate of change statistics by fitting the least squares regression to all the shoreline positions at each transect, from oldest to newest. The findings are depicted in (Fig. 8a and 9), which show the overall incidence of coastal variability as determined by the analysis. The shoreline has positive values associated with accretion and negative values associated with erosion.

The total average LRR shows the cumulative trend of the shoreline for all segments during 31 years (Table 2). The m/yr, respectively. The average level of the entire research region demonstrates that the shoreline from the Mekong River mouth to the Ganh Hao mouth has accretion. The highest accretion distance is 117.06 m, with an average speed of 24.2 m/yr. Meanwhile, the shoreline from Ganh Hao mouth to Ca Mau Cape is retrograding at a pace of -115.5 m/yr, with an annual average speed of -29.49 m/yr.

Figures 8a and 9 display the development based on shoreline position segments recorded using the LRR approach. The analysis also clearly demonstrates that the shoreline displacement varies throughout the studied region. Table 2 and Figures 8b, 8c, 10, 11 show the spatial dynamics of the shoreline through seven divided segments LRR average rates for segments A to G are 0.04 m/yr, 3.59 m/yr, 16 m/yr, 11.03 m/yr, 24.2 m/yr, 7.69 m/yr, and -29.49 (A–G). The overall average EPR rates for all segments show an accretion trend of 0.84 m/yr, 3.75 m/yr, 16.81 m/yr, 11.38 m/yr, 24.29 m/yr, 8.37 m/yr, and -30.11 m/yr for segments A to G, respectively.

The NSM distance values follow the same trend with 25.83 m, 113.45 m, 492.96 m, 352.64 m, 725.16 m, 259.89 m, and -926.37 m, respectively, for segments A to G. The maximum accretion distance (NSM) values are 2471.96 m, 2431.89 m, 2691.64 m, 2688.36 m, 2666.20 m, 2626.66 m and 875.70 m for the segments A to G, respectively, while the maximum accretion EPR rates for the segments in the same order are 80.04 m/yr, 108.76 m/yr, 118.25 m/yr, 107.61 m/yr, 188.66 m/yr, 85.05 m/yr, and 28.35 m/yr.

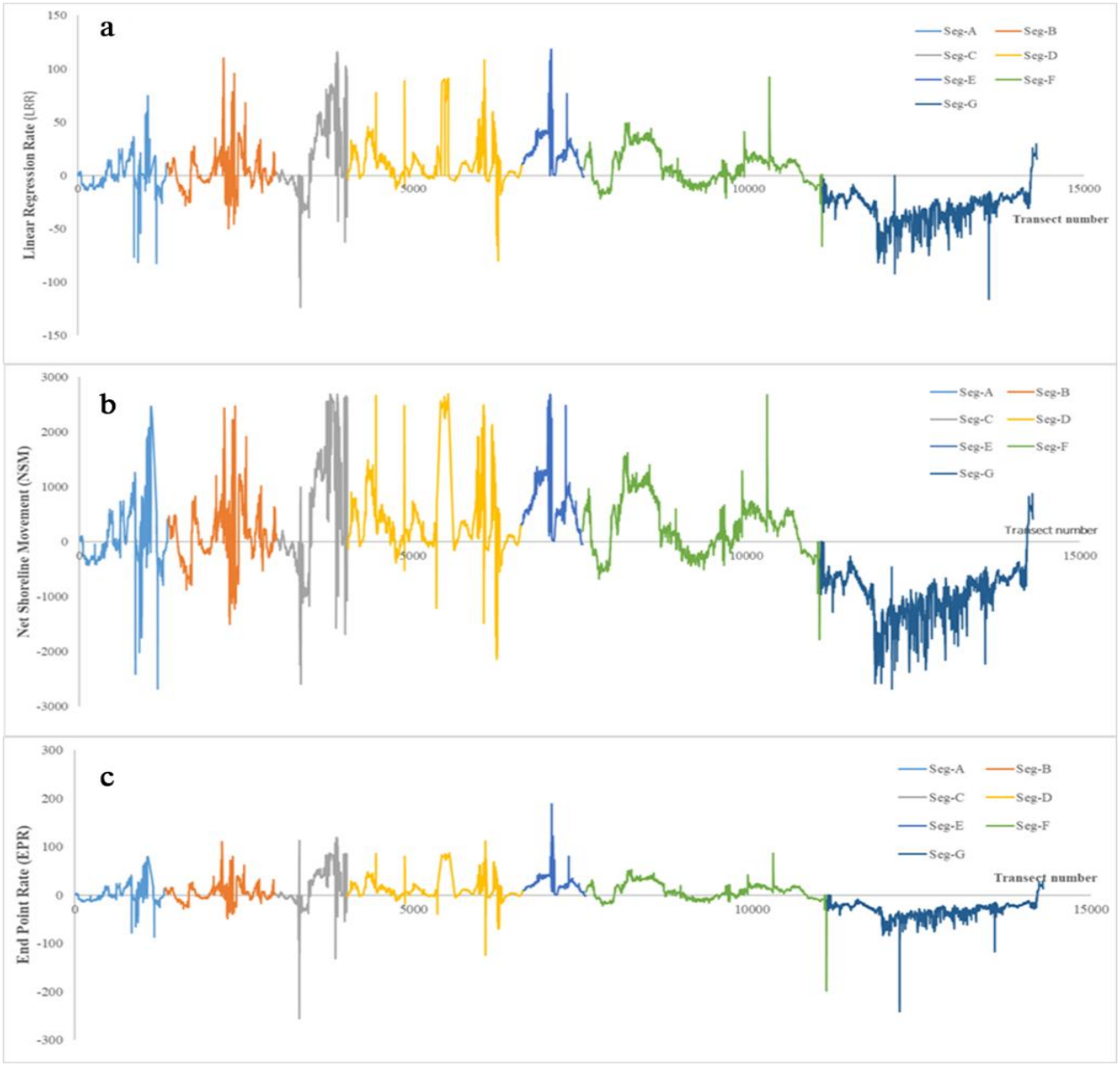

Figure 8. a) The rate of shoreline change (LRR in m/yr), b) Net Shoreline Movement (NSM in m), c) End Point Rate (EPR in m/yr) for the years 1989 to 2020

10.57647/j.ijes.2025.16851

Table 2. Statistical results of LRR (m/yr), NSM (m), EPR (m/yr), and the accretion - erosion area (ha) of the Mekong River mouth and the southern area of the Mekong River mouth for 1989 to 2020

		Category	Seg - A	Seg - B	Seg - C	Seg - D	Seg - E	Seg - F	Seg - G
Statistical results for 1989 to 2020	LRR (m/yr)	Max (m/yr)	74.94	108.19	115.16	106.93	117.06	91.06	29.67
		Min (m/yr)	-82.42	-49.88	-120.98	-79.9	-1.37	-66.07	-115.5
		Average (m/yr)	0.04	3.59	16.00	11.03	24.20	7.69	-29.49
	NSM (m)	Max (m)	2471.96	2431.89	2691.64	2688.36	2666.20	2626.66	875.70
		Min (m)	-2682.33	-1491.45	-2591.08	-2141.52	-48.79	-1777.76	-2653.95
		Average (m)	25.83	113.45	492.96	352.64	725.16	259.89	-926.37
	EPR (m/yr)	Max (m/yr)	80.04	108.76	118.25	107.61	188.66	85.05	28.35
		Min (m/yr)	-86.85	-48.29	-255.76	-118.26	-1.58	-197.79	-241.39
		Average (m/yr)	0.84	3.75	16.81	11.38	24.29	8.37	-30.11
	The accretion - erosion area (ha)	1989-2020 (ha)	-462.7	-347.7	-530.4	-90.094	-4.226	-795.75	-7605.7
			691.49	1422.5	1429.3	2897.3	1502	3249.2	118.277
		Net 1989-2020 (ha)	228.81	1074.8	898.88	2807.2	1497.3	2453.4	-7487.5
Statistical results for 1989 to 1998	NSM (m)	Max (m/yr)	285.74	301.34	306.07	304.69	298.04	304.41	64.15
		Min (m/yr)	-24.84	-164.98	-287.14	-21.38	-6.71	-194.27	-234.10
		Average (m/yr)	9.60	8.90	44.48	16.80	35.30	11.26	-34.60
	EPR (m/yr)	Max (m)	2516.13	2653.47	2695.14	2682.99	2624.46	2680.53	564.86
		Min (m)	-218.71	-1452.79	-2528.45	-188.30	-59.07	-1710.63	-2061.38
		Average (m)	84.57	78.37	391.72	147.97	310.87	99.17	-304.67
	The accretion - erosion area (ha)	1989-1998 (ha)	-146.53	-123.61	-92.23	-82.86	-5.51	-512.70	-2434.13
			314.48	802.99	959.35	828.25	550.03	1429.26	86.81
		Net 1989 - 1998 (ha)	167.94	679.39	867.12	745.38	544.51	916.56	-2347.32
Statistical results for 1998 to 2008	NSM (m)	Max (m)	389.00	2345.15	2633.47	2606.13	2685.86	789.87	720.85
		Min (m)	-2685.30	-2341.39	-1608.01	-260.90	-27.97	-2366.61	-1609.70
		Average (m)	-70.45	-0.47	151.07	86.91	317.01	2.30	-259.30
	EPR (m/yr)	Max (m/yr)	38.44	231.72	260.21	257.51	265.39	78.05	71.23
		Min (m/yr)	-265.33	-231.35	-158.89	-25.78	-2.76	-233.84	-159.05
		Average (m/yr)	-6.96	-0.05	14.93	8.59	31.32	0.23	-25.62
	The accretion - erosion area (ha)	1998-2008 (ha)	-227.69	-326.70	-196.21	-173.18	-0.91	-589.14	-2095.40
			54.67	372.60	474.17	679.91	690.39	640.28	42.82
		Net 1998 - 2008 (ha)	-173.02	45.90	277.95	506.73	689.48	51.13	-2052.57
Statistical results for 2008 to 2020	NSM (m)	Max (m/yr)	220.16	220.11	218.54	225.46	189.16	224.60	70.27
		Min (m/yr)	-196.87	-98.08	-178.60	-209.67	-3.58	-35.74	-197.17
		Average (m/yr)	-1.66	4.22	-2.04	9.50	10.76	13.08	-32.63
	EPR (m/yr)	Max (m)	2632.83	2632.25	2613.53	2696.23	2262.21	2685.92	840.34
		Min (m)	-2354.36	-1172.90	-2135.86	-2507.39	-42.85	-427.39	-2357.91
		Average (m)	-19.90	50.43	-24.44	113.58	128.68	156.37	-390.25
	The accretion - erosion area (ha)	2008-2020 (ha)	-307.16	-177.60	-279.29	-243.87	-11.73	-463.06	-3107.53
			420.30	525.35	239.13	1180.06	275.61	1943.02	27.51
		Net 2008 - 2020 (ha)	113.14	347.74	-40.16	936.19	263.87	1479.97	-3080.03

The maximum erosion distance (NSM) reaches -2682.33 m, -1491.45 m, -2591.08 m, -2141.52 m, -48.79 m, -1777.76 m, and -2653.95 m for the segments A to G, respectively. The maximum erosion EPR rates are -86.85 m/yr, -48.29 m/yr, -255.76 m/yr, -118.26 m/yr, -1.58 m/yr, -197.79 m/yr, and -241.39 m/yr for the same segment in the same order. The results showed that segment G is affected by erosion, other segments are affected by accretion, and

segment C has the strongest accretion with an average NSM distance and EPR rate of 725.16 m and 24.29 m/yr, respectively. Segment G has the strongest erosion, with an average NSM distance and EPR rate of -926.37 m and -30.11 m/yr, respectively.

3.2. Morphological change rates for a short period

3.2.1. *The period from 1989 to 1998*

The rate of change in shoreline position estimated by NSM and EPR approaches throughout this period shows that the Mekong Delta shoreline is primarily due to accretion.
Table 2 and Figures. 12, 13, 14a, 15a show the spatial dynamics of the shoreline through seven divided segments (A–G). The graph shows positive and negative values of EPR rate and distance NSM, which specify accretion or erosion of the shoreline, respectively.
The overall average NSM distance for all segments shows an accretion trend with 84.57 m, 78.37 m, 391.72 m, 147.97 m, 310.87 m, and 99.17 m, respectively, for segments A to segments F. On the other hand, segment G exhibits erosion with an average NSM of -304.67 m. The EPR rate values follow the same trend with 9.60 m/yr, 8.90 m/yr, 44.48 m/yr, 16.80 m/yr, 35.30 m/yr, 11.26 m/yr, and -34.60 m/yr for segments A to G, respectively.
The maximum accretion distance NSM values are 2516.13 m, 2653.47 m, 2695.14 m, 2682.99 m, 2624.46 m, 2680.53 m, and 564.86 m for segments A to G, respectively, while the maximum accretion EPR rates for the segments in the same order are 285.74 m/yr, 301.34 m/yr, 306.07 m/yr, 304.69 m/yr, 298.04 m/yr, 304.41 m/yr, and 64.15 m/yr.

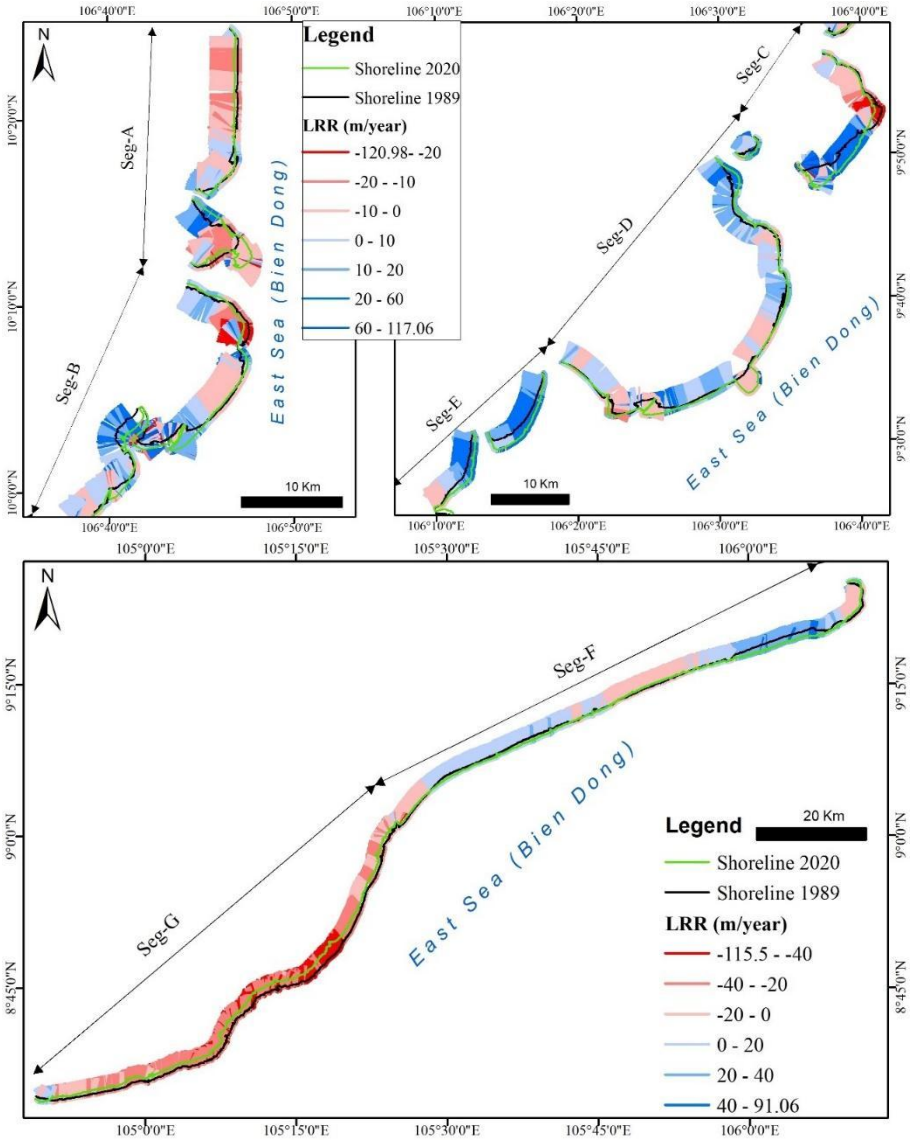

Figure 9. Linear Regression Rate (LRR) of the shoreline change calculated for the time period (1989–2020). Red signifies erosion; blue signifies accretion

10.57647/j.ijes.2025.16851

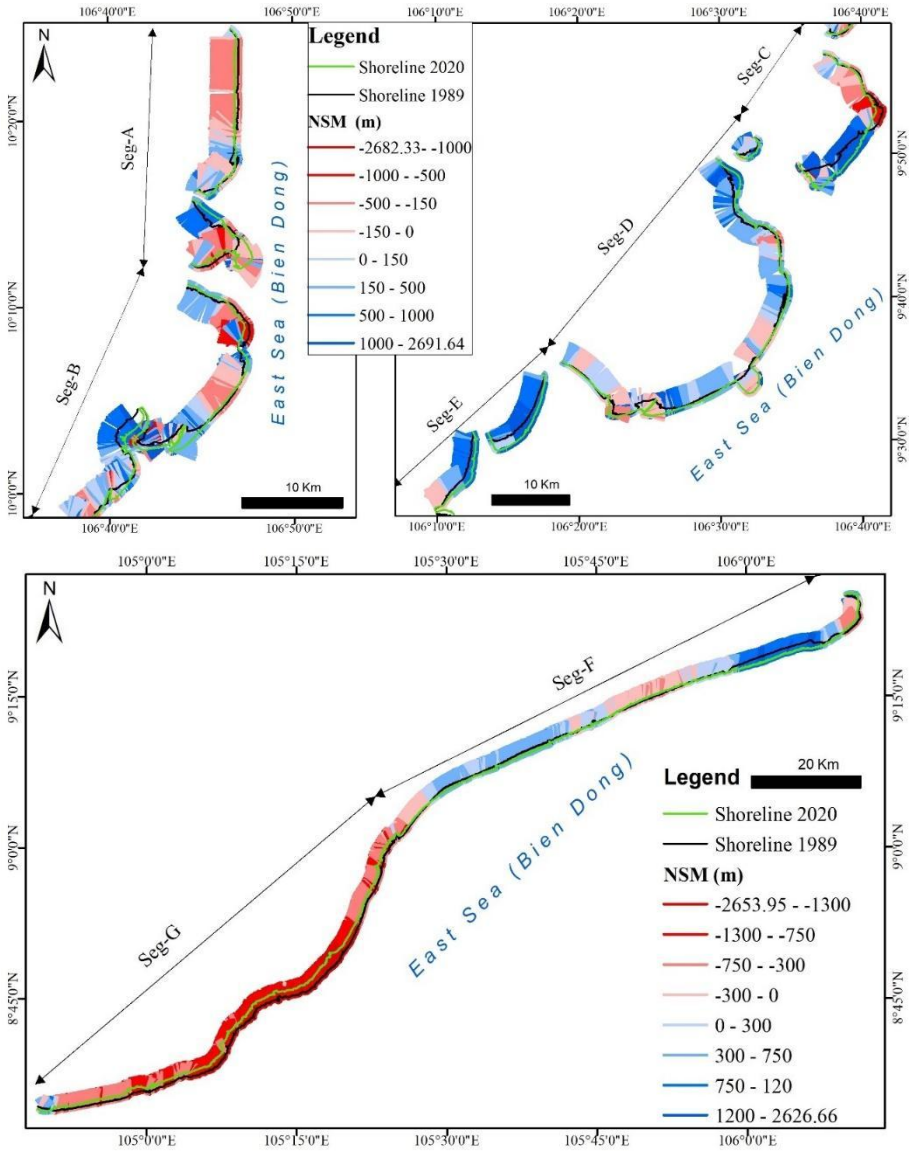

Figure 10. Net shoreline movement (NSM) calculated for the period (1989–2020).Red signifies erosion; blue signifies accretion

The maximum erosion EPR rates reach 285.74 m/yr, 301.34 m/yr, 306.07 m/yr, 304.69 m/yr, 298.04 m/yr, 304.41, and 64.15 m/yr. The erosion distance NSM is 2516.13 m, 2653.47 m, 2695.14 m, 2682.99 m, 2624.46 m, 2680.53 m, and 564.86 m for the same segments in the same order. This suggests that the accretion and erosion rates at the Mekong mouth and the southern part of the Mekong River mouth to Ganh Hao mouth (segments A to F) are accretions. Segment C is the strongest accretion with an average NSM distance and EPR rate of 391.72 m and 44.48 m/yr, respectively. While the rate of accretion and erosion from Ganh Hao mouth to Ca Mau Cape (segment G) is the strongest erosion, with an average NSM distance and EPR rate of -304.67 m and -34.6 m/yr, respectively, as shown in Table 2.

3.2.2. *The period from 1998 to 2008*

During the period from 1998 to 2008, overall average EPR rates for all segments show erosion and accretion in alternating segments with -6.96 m/yr, -0.05 m/yr, 14.93 m/yr, 8.59 m/yr, 31.32 m/yr, 0.23 m/yr, and -25.62 m/yr for segments A to G, respectively (Table 2 and Figs. 12, 13, 14a, 15a). The NSM distance values follow the same trends with -70.45 m, -0.47 m, 151.07 m, 86.91 m, 317.01 m, 2.30 m, and -259.30 m, respectively, for segments A to G. The maximum erosion distance (NSM) values are -2685.30 m, -2341.39 m, -1608.01 m, -260.90 m, -27.97 m, -2366.61 m, and -1609.70 m for the segments A to G, respectively (Table 2 and Figs. 12, 13, 14a, 15a). While the maximum erosion EPR rates for the same segments are in the same order as -265.33 m/yr, -231.35 m/yr, -158.89 m/yr, -25.78

m/yr, -2.76 m/yr, -233.84 m/yr, and -159.05 m/yr. The maximum accretion distance (NSM) reaches 389.00 m, 2345.15 m, 2633.47 m, 2606.13 m, 2685.86 m, 789.87 m, and 720.85 m for segments A to G, and the maximum accretion EPR rates are 38.44 m/yr, 231.72 m/yr, 260.21 m/yr, 257.51 m/yr, 265.39 m/yr, 78.05 m/yr, and 71.23 m/yr for the same segments in the same order (Table 2 and Figs. 12, 13, 14a, 15a).

The results showed that during the period (1998–2008), the morphological changes in the coastal shoreline at the Mekong River mouth area decreased as compared to the previous period (1989–1998), with segments A and G affected by erosion. Segments B and F are affected by erosion or accretion, which is not significant (less than ± 1 m/yr for EPR rate), and other segments are affected by accretion. Segment G has the strongest erosion, with an average NSM distance and EPR rate of -259.3 m and -25.62 m/yr, respectively. Segment E is the strongest accretion, with an average NSM distance and EPR rate of 317.01 m and 31.32 m/yr, respectively.

3.2.3. *The period from 2008 to 2020*

During the period from 1998 to 2008, the overall maximum accretion distance (NSM) for all segments is 2632.83 m, 2632.25 m, 2613.53 m, 2696.23 m, 2262.21 m, 2685.92 m, and 840.34 m for segments A to G, respectively (Table 2 and Figs. 12, 13, 14a, 15a).

The maximum accretion EPR rates for the segments are in the same order as 220.16 m/yr, 220.11 m/yr, 218.54 m/yr, 225.46 m/yr, 189.16 m/yr, 224.60 m/yr, and 70.27 m/yr.

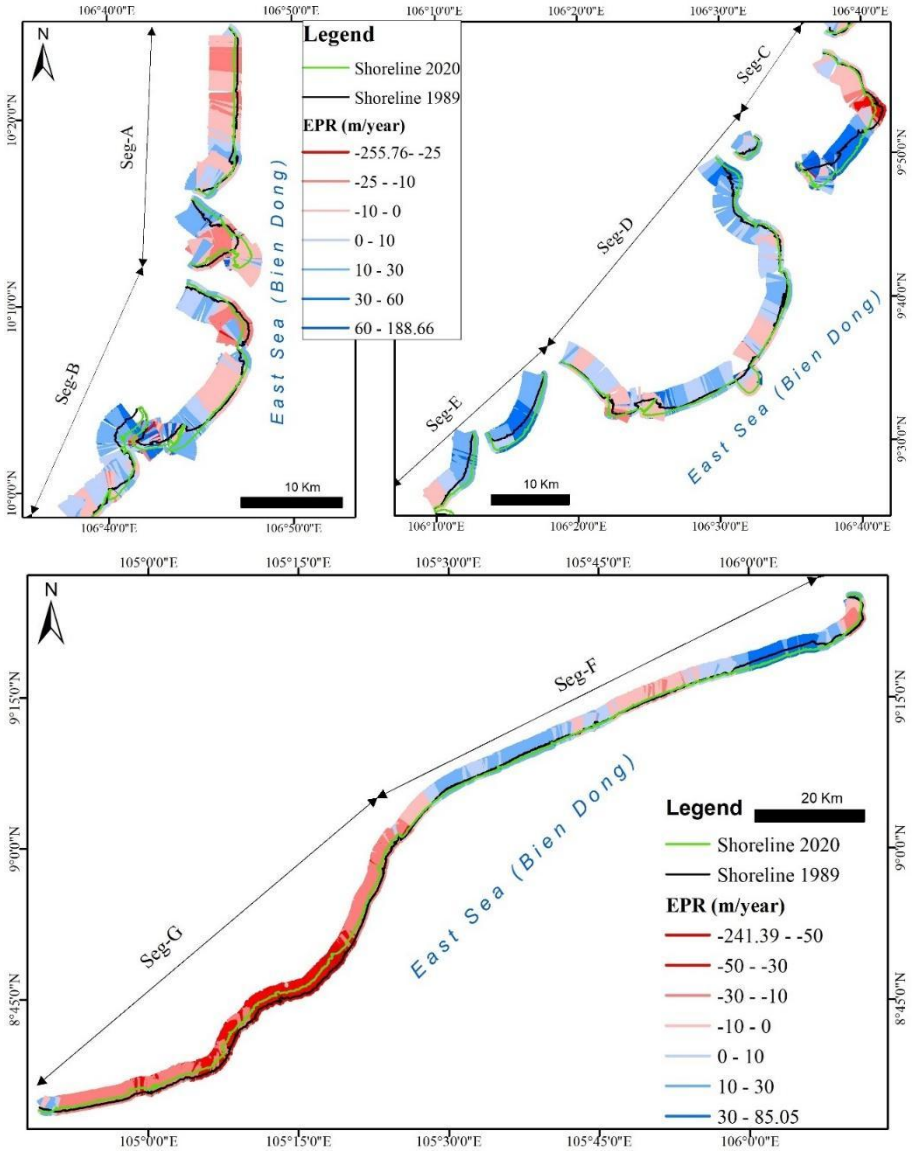

Figure 11. End point rate (EPR) calculated for the period (1989–2020). Red signifies erosion; blue signifies accretion

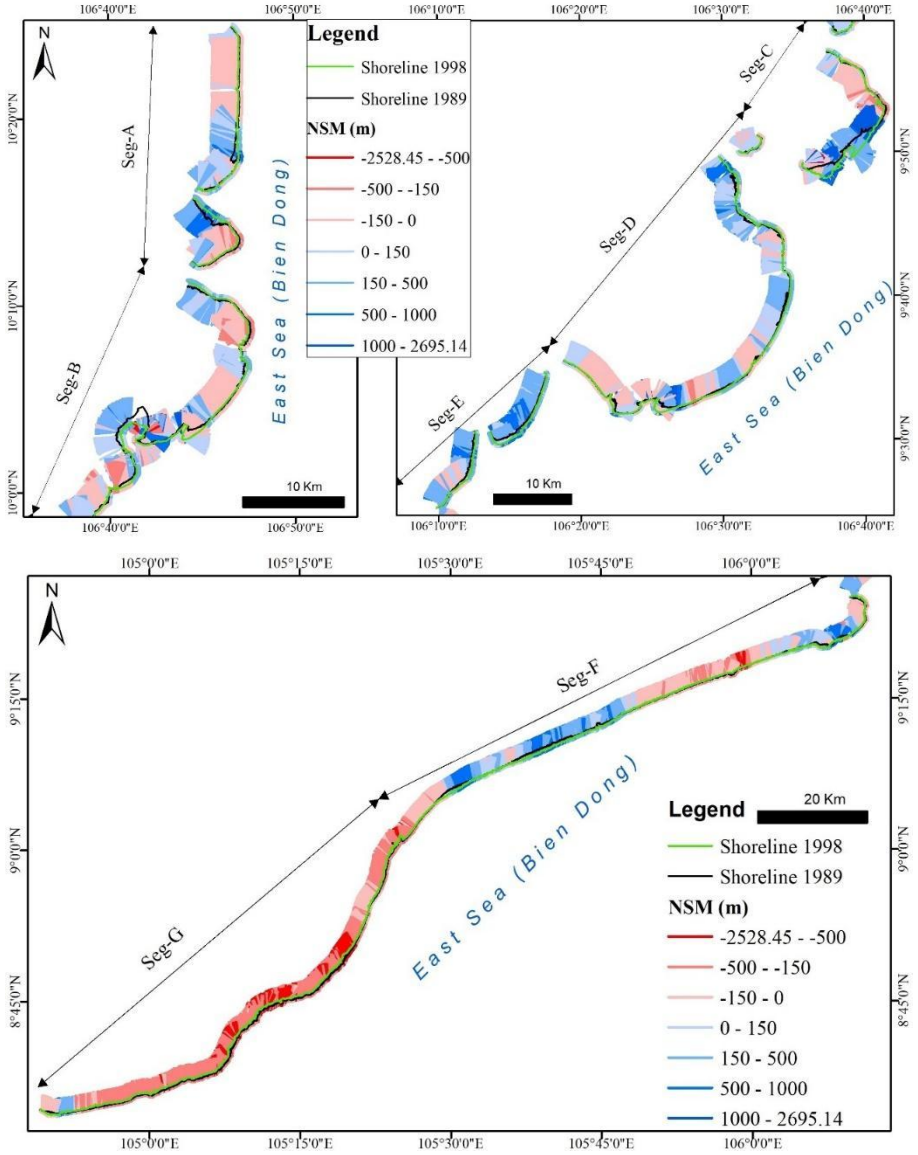

Figure 12. Net Shoreline Movement (NSM) calculated for the time period (1989–1998). Red signifies erosion; blue signifies accretion

The maximum erosion EPR rates reach -196.87 m/yr, -98.08 m/yr, -178.60 m/yr, -209.67 m/yr, -3.58 m/yr, -35.74 m/yr, and -197.17 m/yr for segments A to G, respectively (Table 2 and Figs. 12, 13, 14a, 15a). While the maximum erosion distance (NSM) values are -2354.36 m, -1172.90 m, -2135.86 m, -2507.39 m, -42.85 m, -427.39 m, and -2357.91 m for the same segments in the same order. The average (NSM) distance for all segments shows erosion and accretion in alternating segments of -19.90 m, 50.43 m, -24.44 m, 113.58 m, 128.68 m, 156.37 m, and -390.25 m for segments A to G, respectively. The EPR rates for the same trends were -1.66 m/yr, 4.22 m/yr, -2.04 m/yr, 9.50 m/yr, 10.76 m/yr, 13.08 m/yr, and -32.63 m/yr, respectively, for segments A to G (Table 2 and Figs. 12, 13, 14a, 15a).

During this period, the average EPR and NSM in the Mekong River mouth area showed a decrease compared to the two previous periods. The average EPR and NSM at the Mekong River mouth were 4.15 m/yr and 49.67 m, respectively. The results showed that segments A, C, and G are affected by erosion, and other segments are affected by accretion. Segment G (from Ganh Hao mouth to Ca Mau Cape) has the strongest erosion, with an average NSM distance and EPR rate of -390.25 m and -32.63 m/yr, respectively. Segment F (the southern part of the Mekong River mouth to Ganh Hao mouth) is the strongest accretion with an average NSM distance and EPR rate of 156.37 m and 13.08 m/yr, respectively, as shown in Table 2.

3.3. Area change

3.3.1. *The Mekong Estuary area*

Human activities since the 1970s, including hydropower dam construction, illicit sand mining, groundwater

extraction-induced subsidence, and declining coastal mangrove protection, have adversely affected the Mekong Delta's coastal region.

Based on the shoreline in the research region of the Mekong estuary, it witnessed alternating erosion and accretion (Fig. 20) from 1989 to 2020. Here, the accretion area is larger than the erosion area. Table 2 and Figure 20 reveal that the Mekong estuary, which has a length of more than 270 km (in the research area of 2020), has poor accretion in all seven estuaries.

The rate of change of the erosion - accretion area changes at segment B (Ba Lai): from 1989 to 1998, the area changed from 679.39 hectares (ha) to 123.61 ha of erosion and 802.99 ha of accretion. From 1998 to 2008, the erosion area grew while the accretion area shrank, resulting in a 45.9 ha balance of erosion and accretion. From 2008 to 2020, reduce the erosion area to 177.6 ha while increasing the accretion area to 525.35 ha, resulting in an increase in the changed land area to 347.74 ha (Fig. 23, Table 2).

Segment D's (Cung Hau-Dinh An mouth) transformed land area is 745.38 ha (1989–1998), 506.73 ha (1998–2008), and 936.19 ha (2008–2020). The erosion and accretion areas are both increasing here, with erosion areas changing by -82.86, -173.18, and -243.87 ha, respectively, for 1989–1998, 1998–2008, and 2008–2020. While the accretion area has changed by 828.25, 679.91, and 1180.06 ha, respectively, for 1989–1998, 1998–2008, and 2008–2020 (Fig. 23, Table 2). During the period 2008–2020, when Duyen Hai's thermal power station was developed, they encroached on the sea to make a wharf, leading to a significant increase in the accretion area (Fig. 21a).

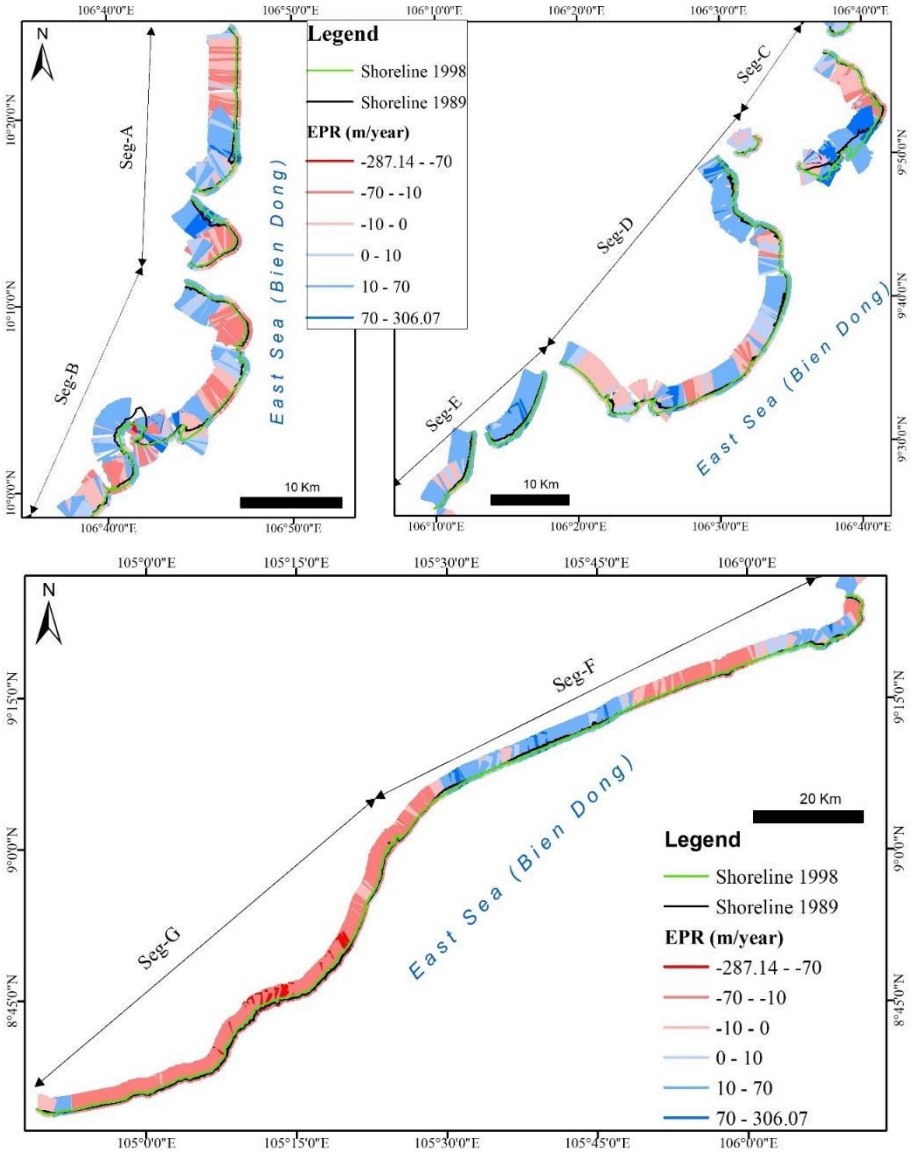

Figure 13. End point rate (EPR) calculated for the time period (1989–1998). Redsignifies erosion; blue signifies accretion

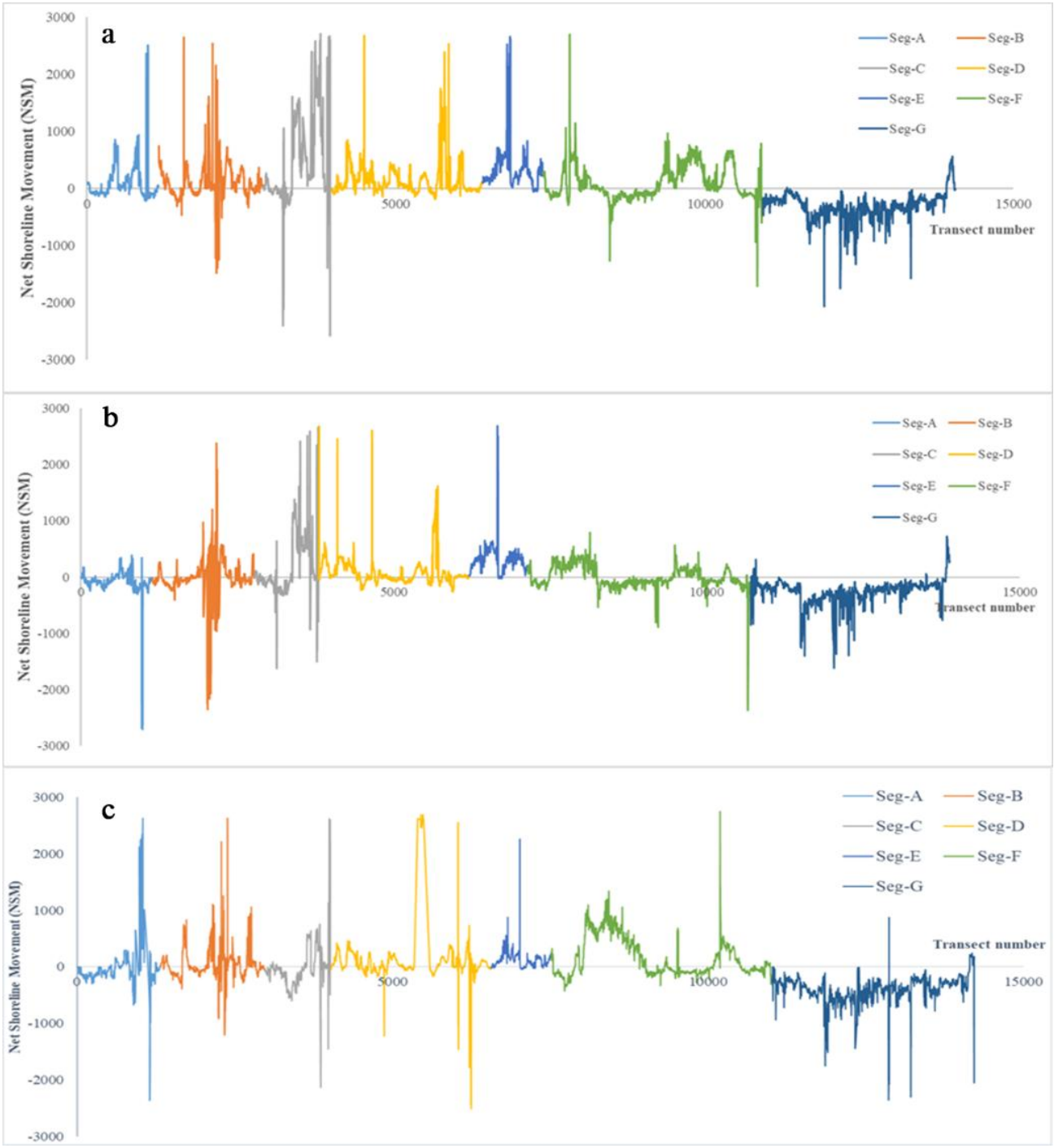

Figure 14. Net Shoreline Movement (NSM in m) for the years. a) from 1989 to 1998; b) from 1998 to 2008; c) from 2008 to 2020

Table 2, segment E (Tran De mouth), it is evident that erosion has been minimal across all three stages, resulting in a total degraded land area of 4.226 hectares from 1989 to 2020. The shoreline is mostly accretion, with 544.51 ha of changed land (1989–1998), increasing to 689.48 ha (1998–2008), and just 263.87 ha (2008–2020). This demonstrates that, although the erosion area does not increase, the accretion area decreases (Fig. 23). Unless otherwise noted, from 1998 to 2008, the erosion area was greater than the accretion area at the Tieu mouth and Dai mouth (segment A), resulting in a loss of 173.02 ha. From 1989 to 1998, the area of accretion - erosion was 146.53 ha and 314.48 ha, respectively, and increased to 307.16 ha and 420.30 ha in the period 2008 to 2020 (Fig. 23 and Table 2). The survey results show that, at Thua Duc Beach (Dai mouth), the area north of the estuary has accretion and erosion in the south. To the north of the Dai mouth, a sand dune located far from the shore (detailed in Section 4), now

10.57647/j.ijes.2025.16851

connected to the mainland (Fig. 21b), is also reinforced by engineering works (Fig. 21c); however, the engineering structures are still short (~200 m) and limited. In segment C (Ham Luong-Co Chien mouths), through three stages, the erosion area increases by 92.23 ha, 196.21 ha, and 279.29 ha, respectively. Whereas the accretion area decreases by 959.35 ha, 474.17 ha, and 239.13 ha, respectively. The land area changes from accretion (1989–1998) to erosion (2008–2020). From 2008 to 2020, the area of erosion land was larger than that of accretion (the area of land lost over this period was -40.16 ha) (Fig. 23, Table 2). The survey results at the Ham Luong mouth showed that there was an erosion phenomenon that must be reinforced by an embankment with structures (Fig. 21d). Moreover, erosion - accretion is stronger in the Co Chien mouth, and the features of this area are mostly wetlands and mangroves, making the employment of structural solutions to prevent erosion - accretion problematic. Instead, they utilize intermittent geotubes to decrease the probability of erosion and accretion here (Fig. 21e).

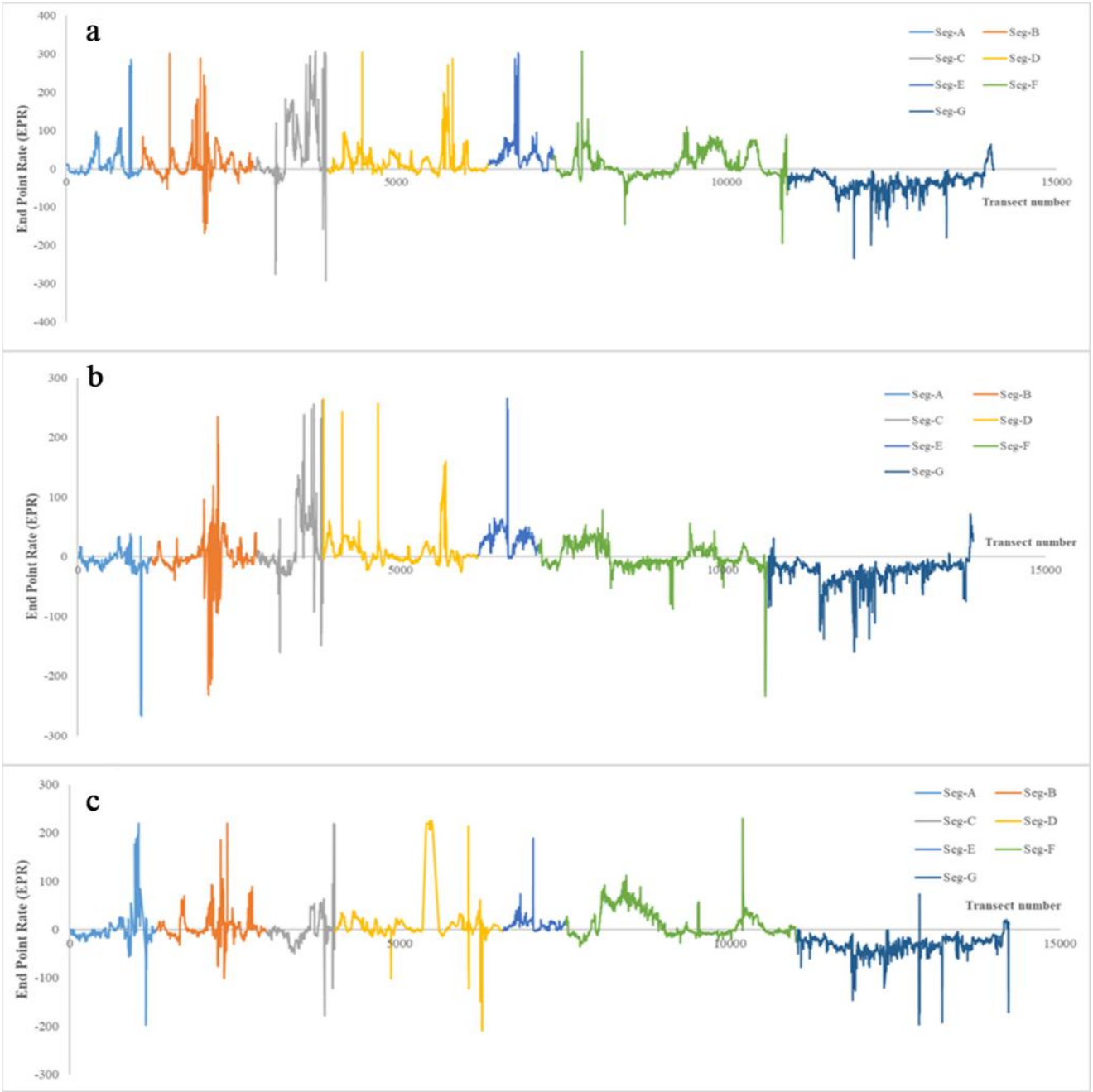

Figure 15. End Point Rate (EPR in m/yr) for the years. a) from 1989 to 1998; b)from 1998 to 2008; c) from 2008 to 2020

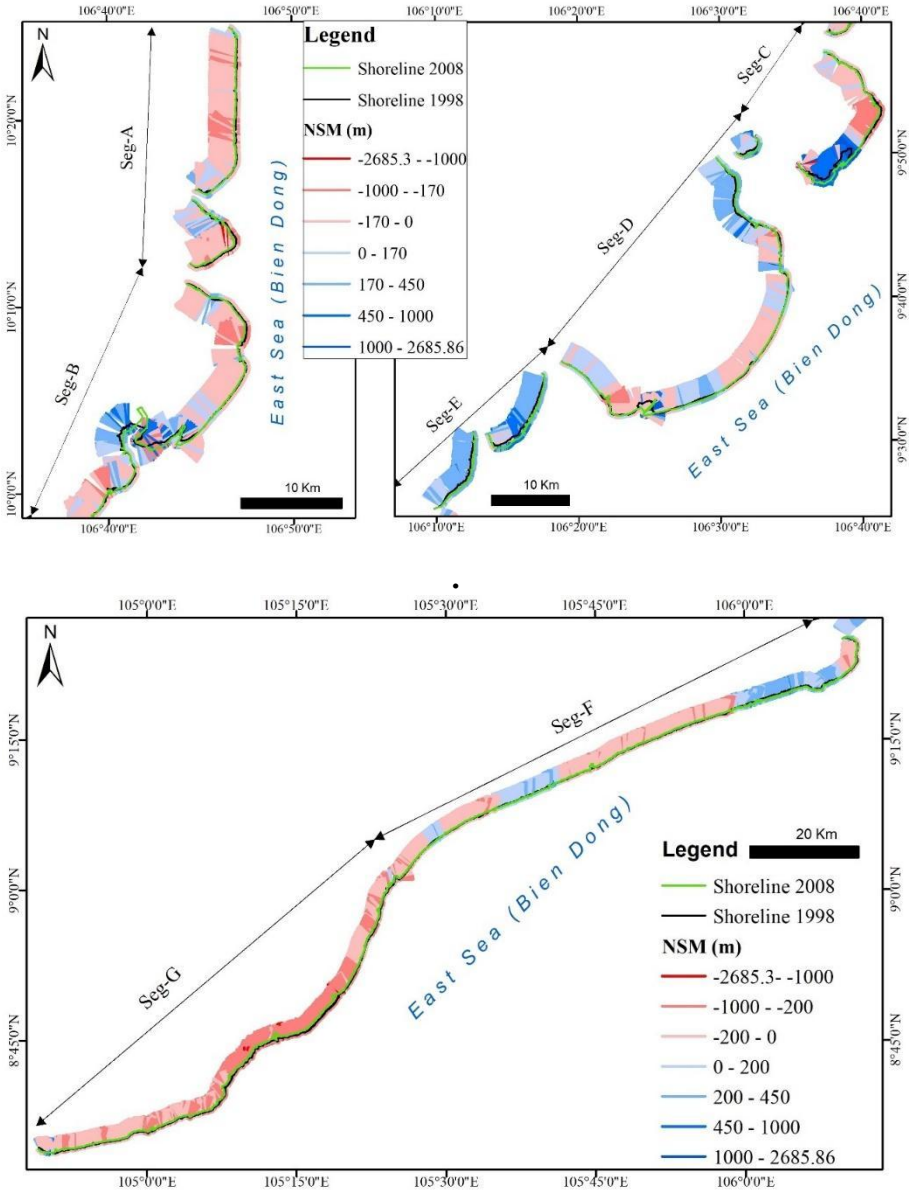

Figure 16. Net Shoreline Movement (NSM) calculated for the time period (1998–2008). Red signifies erosion; blue signifies accretion

3.3.2. *The southern area of the Mekong River mouth*

The shoreline of the area south of the Mekong Estuary can be divided into two segments: segment 1 from My Thanh mouth to Ganh Hao mouth and segment 2 from Ganh Hao mouth to Ca Mau Cape. This area has a length of around 230 kilometers. This is the most dynamic location in the region, with rates of erosion and accretion varying at rates of up to 240 ha/yr and around 150 ha/yr, respectively (Table 2).

The rate of change of the area of erosion and accretion is not balanced in the region extending from the My Thanh mouth to the Ganh Hao mouth (segment F, Fig. 22). The ratio of the accretion rate to the erosion rate is three times greater in the period (1989–1998) and more than four times higher in the period (2008–2020), respectively, increasing the accretion land area to 916.56 ha and 1479.97 ha. In the period 1998–2008, erosion and accretion rates were more evenly distributed, with an overall change in land area of 51.13 ha (Fig. 23, Table 2). The shoreline in this area changes from straight to undulating (Li et al., 2017) which can be seen in the actual photo (Fig. 21f) and Google Earth photo (Fig. 21g).

The bank from Ganh Hao mouth to Ca Mau Cape (segment G, Fig. 22) is in erosion at an erosion rate of over 200 ha/yr, in contrast to the area from My Thanh mouth to Ganh Hao mouth, which is in accretion. The land area erosion along the 110 km-long bank is 2434.13 ha, 2095.4 ha, and 3107.53 ha, respectively, for 1989–1998, 1998–2008, and 2008–2020. The accretion rate, which is less than 10 ha per year near Ca Mau Cape and tends to steadily decline over time, is now 8.68, 3.89, and 2.12 ha per year, respectively,

for 1989–1998, 1998–2008, and 2008–2020 (Fig. 23, Table 2). According to statistics, the shoreline of the study area has been retrograded in the Mekong Delta, with a total length of more than 260 kilometers (accounting for about 52.69% of the shoreline of the study area). The accretion shoreline is about 236 kilometers long (accounting for 47.3% of the shoreline in the study area). The Mekong Delta has seen significant erosion and accretion during the past ten years (phase 3: 2008–2020). It is estimated that 450–500 acres of land are lost to erosion and accretion annually.

The analysis of uncertainty in this study indicates a maximum annualized uncertainty of ±0.58 m per year using the best estimate. This highlights a significant level of uncertainty in the measurements and predictions, which may arise from various sources such as measurement techniques and data quality. It underscores the need for the development of more accurate and precise methodologies for studying coastal erosion and deposition. Additionally, the study emphasizes the importance of creating comprehensive coastal management plans to address issues of erosion and deposition. Such plans would be invaluable for local self-government (LSG) departments, enabling them to identify impacts and implement climate change adaptation and mitigation strategies to preserve the coast.

4. Discussions

This study used three statistical approaches (Table 2) to estimate shoreline change rates, namely LRR calculates the rate of change of the shoreline over each year. EPR: calculate the shoreline moved between the oldest and newest times. NSM: the distance between the oldest and latest shorelines. These applications are considered excellent markers for shoreline change analysis.

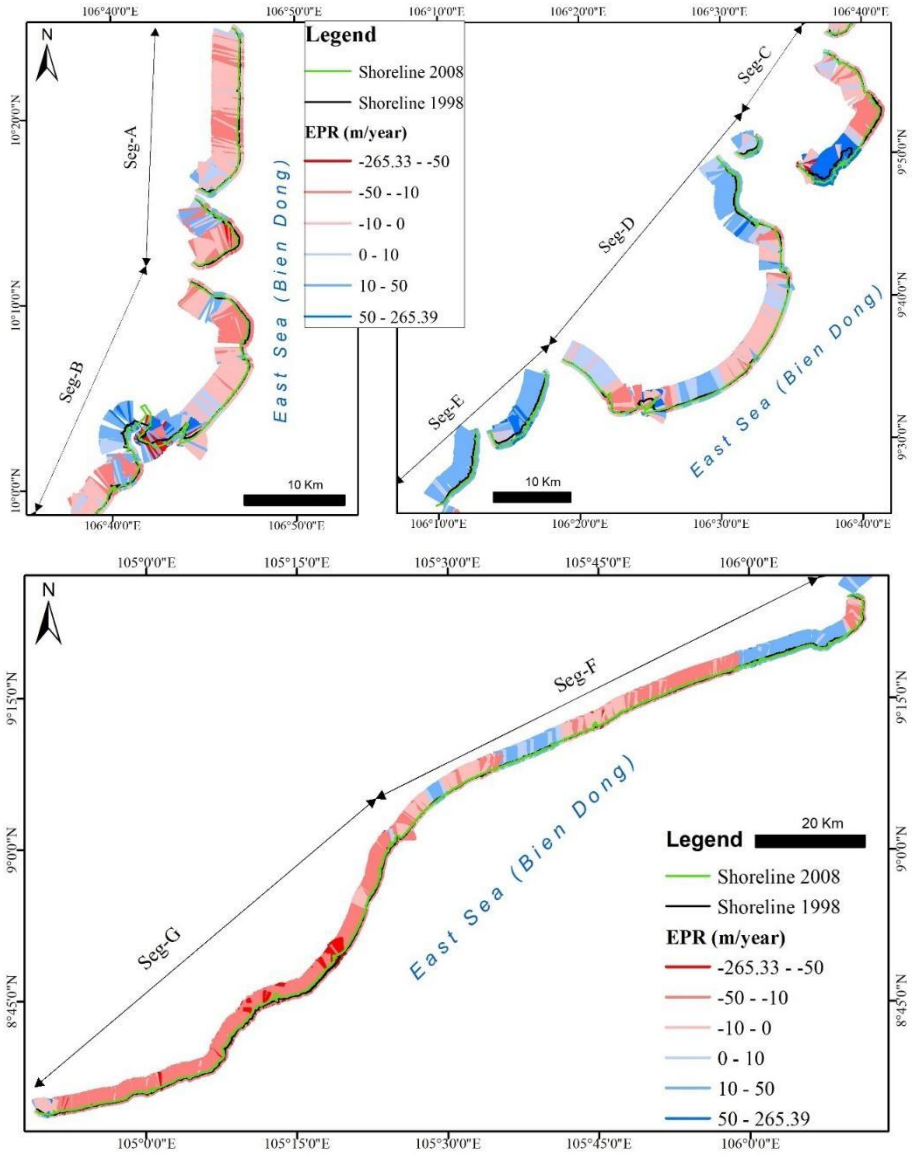

Figure 17. End point rate (EPR) calculated for the time period (1998–2008). Redsignifies erosion; blue signifies accretion

10.57647/j.ijes.2025.16851

Between 2000 and 2020, the coastline of the Mekong Delta experienced substantial changes, with erosion rates averaging 29.49 m/yr and accretion rates of up to 24.2 m/yr in certain areas of the river mouth. The findings revealed that the research region saw substantial changes, such as accretion and erosion, over the period studied. The findings reveal both positive and negative impacts, with accretion indicating land gain and erosion reflecting land loss. This result will serve integrated coastal zone management in the study area.

4.1. Area changes in the Mekong Delta

Through two surveys in July 2022 and February 2023, we found that the coast of the Mekong Delta is mainly mangrove forest and is being changed very strongly. Some sections of the shore were retrograde, threatening dozens of coastal houses if not reinforced in time (Fig. 24 a-c). In the landslide area, there is almost no protective forest to block waves and wind. At present, only a temporary embankment of sandbags and soil is needed to prevent water from overflowing into residential areas (Fig. 24a). This is a temporary solution that has been applied effectively in some provinces in the short time such as Nam Dinh and Thua Thien Hue provinces. Therefore, in addition to coastal afforestation, it is necessary to have concrete works to break waves, reduce landslides, and keep dikes. The example, on the coast of Tien Giang province, initially appeared as a small sandbar about 3km east of the mainland (only exposed at low tide) in the early 1990s, gradually developing (due to accretion) to form a small island (with growing vegetation).

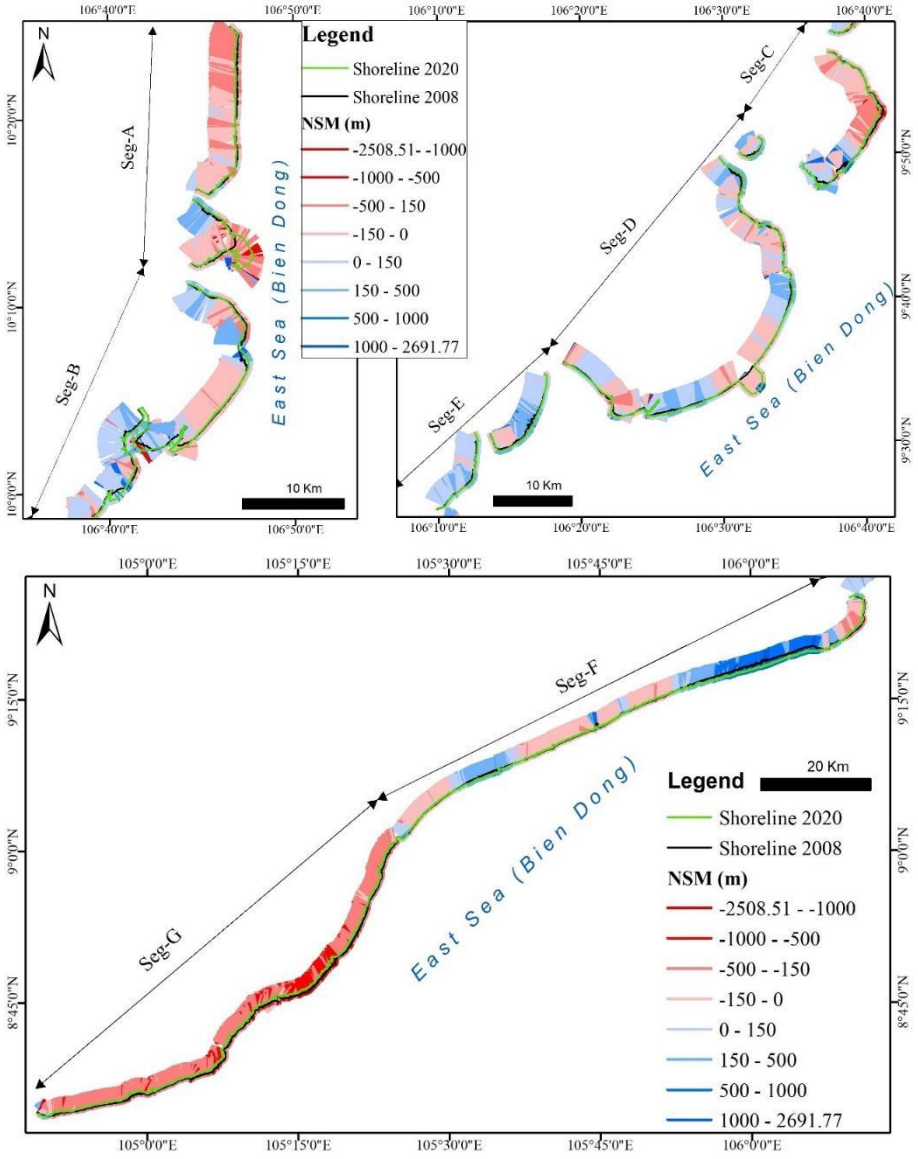

Figure 18. Net Shoreline Movement (NSM) calculated for the time period (2008–2020). Red signifies erosion; blue signifies accretion

10.57647/j.ijes.2025.16851

Around 2015, it developed and attached to the mainland to form a land area of more than 400 ha (Fig. 25a). The shorelines of Ben Tre, Tra Vinh, and Soc Trang provinces also clearly reflect the views of Li et al., (2017) (Fig. 25 b-e). The mechanism of coastal alluvial deposition is explained by the fact that when the sediments from upstream flow into the delta, some of it overflows into the floodplain and most of the rest flows into the sea (Li et al., 2017). It produced murky waters around a coast about 30 kilometers wide. This is believed to have been an effective soft wall protecting the Mekong Delta coast for the past 3,000 years. When seawater contains silt at the coast, it will reduce the impact of waves from the distant sea on the shore. However, the number of alluvial deposits has steadily decreased from the Mekong River to the Mekong Delta over the past 30 years. The sediment load of the Vietnamese Mekong Delta was significantly reduced from 160 Mt/yr in the pre-dam period (Kondolf et al., 2014; Meade, 1996) to 40 Mt/yr in 2012–2013 (Nowacki et al., 2015). There are several reasons for the sediment reduction, but the most notable is the construction of a succession of reservoirs and hydroelectric dams upstream (Bravard et al., 2013; Ha et al., 2018). In river water, at the top are fine alluvial particles, and at the bottom are sand and gravel. When the current is normal, the water carries silt, sand, and gravel downstream. But hydroelectric power plants under construction will hinder this process. The dam on the Mekong will use the river in front of the dam to form a reservoir about 90–100 kilometers long. Typically, dams are built with bottom outlets, but their effectiveness has not been proven. Upon reaching the lake, the water flow significantly decelerates, causing a portion of the sediment to settle in the reservoir and sand outlet. During drainage, it becomes impossible to discharge all the sediment accumulated within the dam.

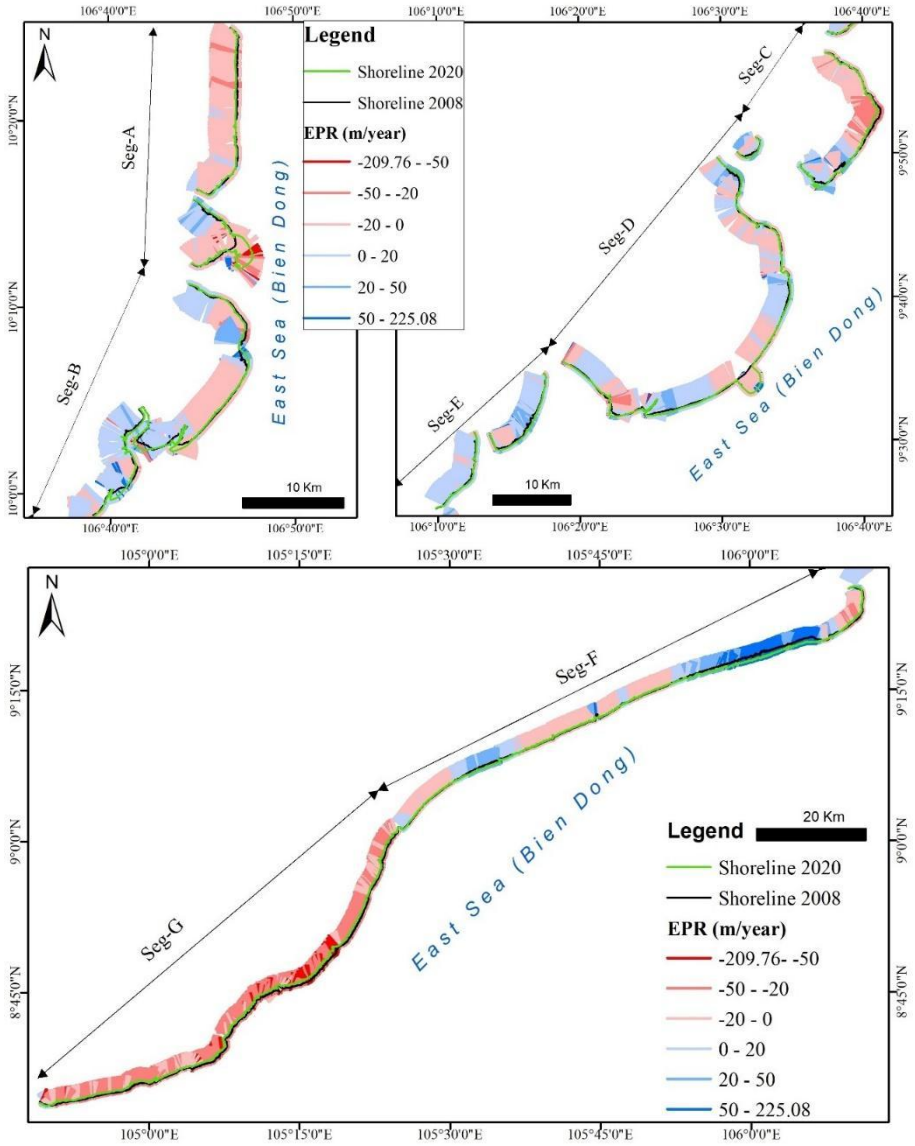

Figure 19. End point rate (EPR) calculated for the time period (2008–2020). Red signifies erosion; blue signifies accretion

10.57647/j.ijes.2025.16851

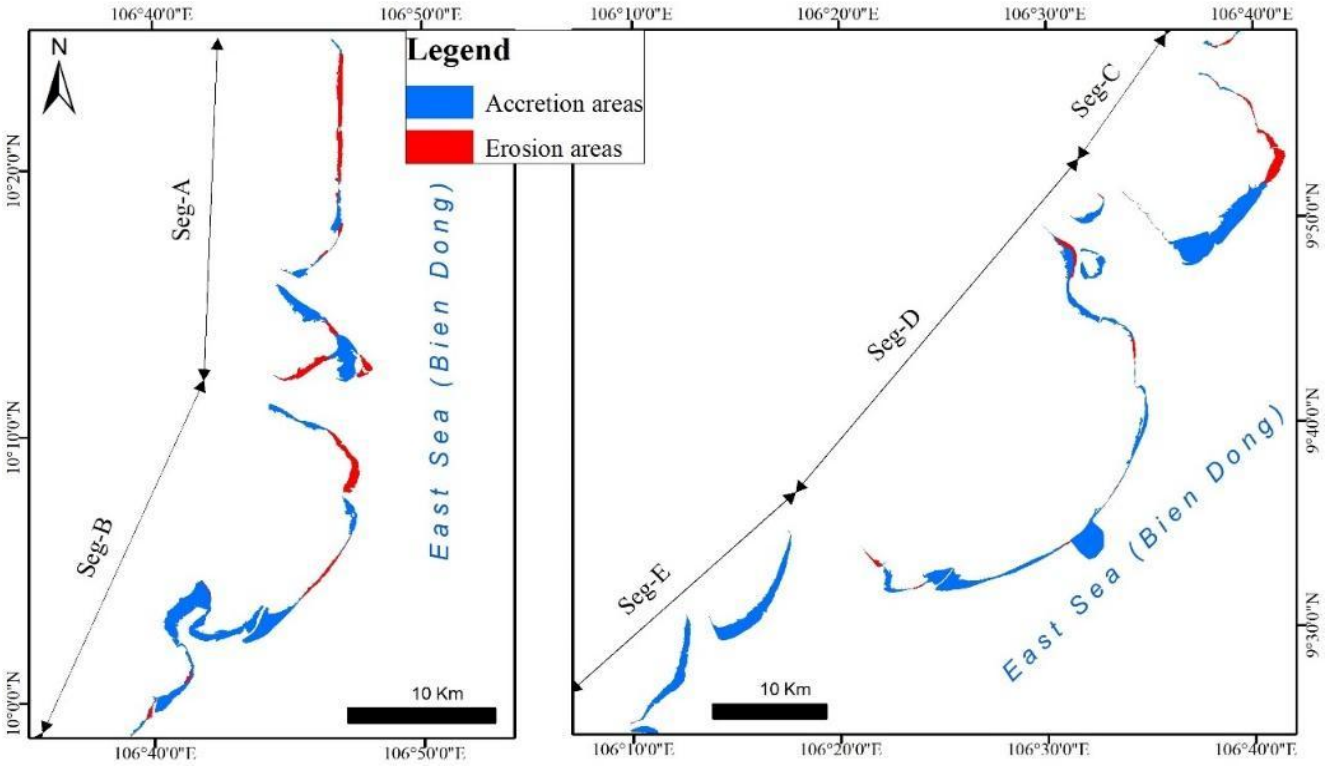

Figure 20. The accretion - erosion area in the Mekong estuary area between theyears 1989 and 2020

In this study, we use Landsat (Landsat 5 TM, Landsat 8 OLI) and Google Earth images to examine the shoreline from the Tieu mouth to Ca Mau Cape between 1989 and 2020. Every study reveals the same erosion - accretion pattern. Our research indicates that shoreline accretion is mostly present from the Tieu mouth to the My Thanh mouth (Mekong River mouth). Mostly accretion is from My Thanh to the Ganh Hao mouth, and major erosion is from the My Thanh mouth to the Ca Mau Cape. Wang et al., (2011) examined the spatial and temporal changes in sediment loads at five upstream stations of the Mekong and found that the temporal variation does not always align with fluctuations in water discharge. Besides water flow, there are many other factors that are also seriously affecting the sediment load. Large-scale sediment mining in the lower basin is one such factor.

The Mekong Delta is experiencing delta subsidence, which worsens the alluvium shortage. Due to the sediment being deposited in the places where the delta is subsiding, the amount of alluvium that is being carried to the sea will continue to decline. The erosion will be more severe, and the form of the delta will alter as a result of the sea level rise and subsidence of the delta side.

The dynamics of the shoreline, notably the transfer of sediment, are greatly influenced by ocean waves. The Mekong Delta's shoreline region has two distinct wind seasons each year: the SW Monsoon, May to October and the NE Monsoon, November to April the following year. The Mekong Delta's wave regime and wind regime are perfectly compatible with one another.

At the base of the protective forest, nearly vertical cliffs have been created by coastal erosion. The impact of the waves on the coast is minimal when the tide is low since the waves are modest. These coastal walls will be immediately impacted by the shock energy of the waves as the tide rises and the waves get bigger and stronger, striking the coast. Not only excavating the bank wall but also creating toe erosion, making the erosion process faster and faster.

Today, the impact of climate change, extreme weather, and sea level rise is changing the dynamic regime of the coastal strip in the Mekong Delta. The erosion and accretion of the coastal strip will increase due to climate change and sea level rise. Once the 30-kilometer-thick alluvial strip is depleted, the mangroves no longer have their protective barrier. The sea dike in the Mekong Delta is seen as the final line of defense against the effects of the sea on production processes, infrastructure, and coastal residents. The Mekong Delta sea dike, however, is constructed on soft ground, has a limited load-carrying capacity, and has a slow consolidation rate. Clay, silt, and sandy soils, which are typical dyke soils and contain a lot of organic matter, have a low capacity to withstand waves. The dike sections are located directly on the sea due to the erosion and

degradation of mangrove forests, leading to the dike not being able to prevent natural disasters from storm surges and high tides. Mangroves are being weakened by inadvertently turning coastal seawall strips into a barrier between the sea and the forest. As mangroves degrade, mangrove protection is no longer guaranteed. It can be said that the cause of the erosion of the Mekong Delta has been identified. The primary causes are the insufficient transport of alluvium from the Mekong River downstream and the construction of sea walls and coastal zone engineering, resulting in detrimental effects. At the same time, land subsidence, climate change, and sea level rise are exacerbating adverse impacts on coastal mangroves. The consequences of coastal erosion in the Mekong Delta are increasingly severe, complex, and difficult to control. If coastal erosion is not stopped, about 90% of the Mekong Delta will be affected if the seawall system and coastal mangroves cannot withstand the negative impacts of the ocean submerged in seawater in the late 21st century (Boretti, 2020).

Figure 21. a) Thermal power station Duyen Hai[1]. b) the sand dune has connected tothe mainland; c) the engineering works at Thua Duc beach; d) the beach at Ham Luong mouth with the engineering works; e) The Co Chien mouth used geotube to prevent erosion; f) an actual photo of the shoreline undulating (photo by the Bui Minh Quan), g) a Google Earth photo showing the shoreline undulating (photo by Google Earth)

[1] https://www.tpcduyenhai.com.vn/

10.57647/j.ijes.2025.16851

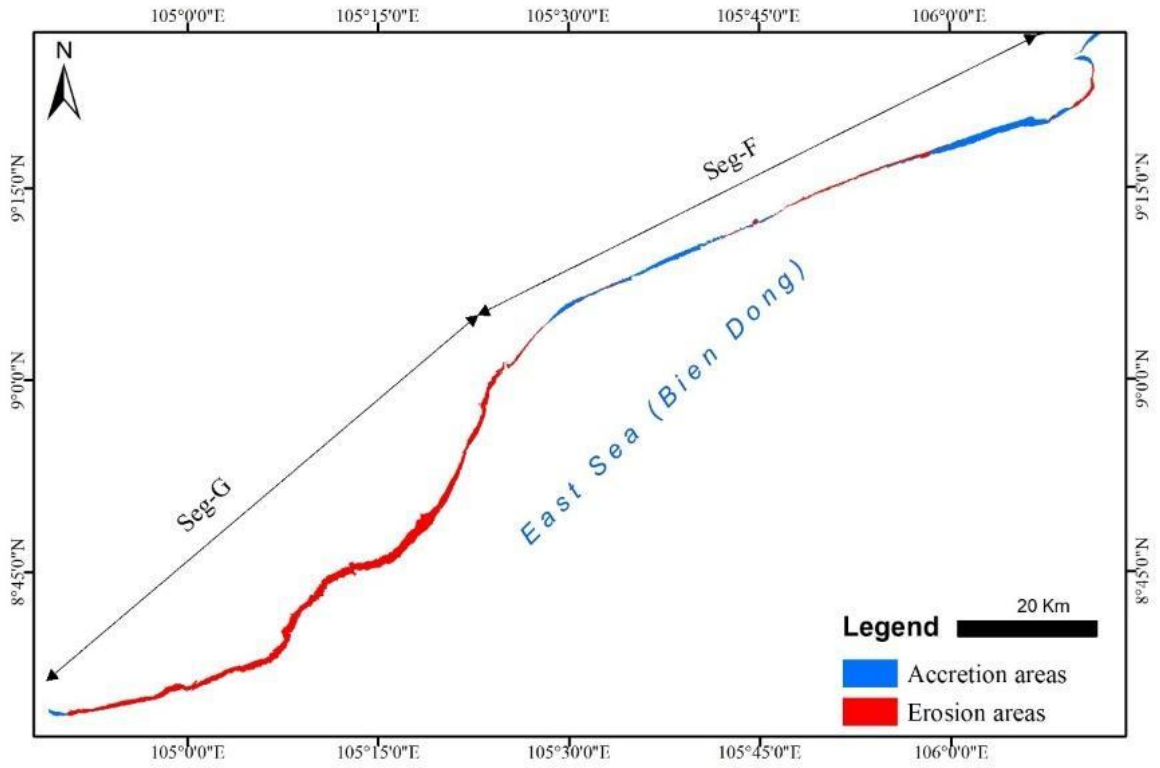

Figure 22. The accretion - erosion area in the southern area of the Mekong Rivermouth between the years 1989 and 2020

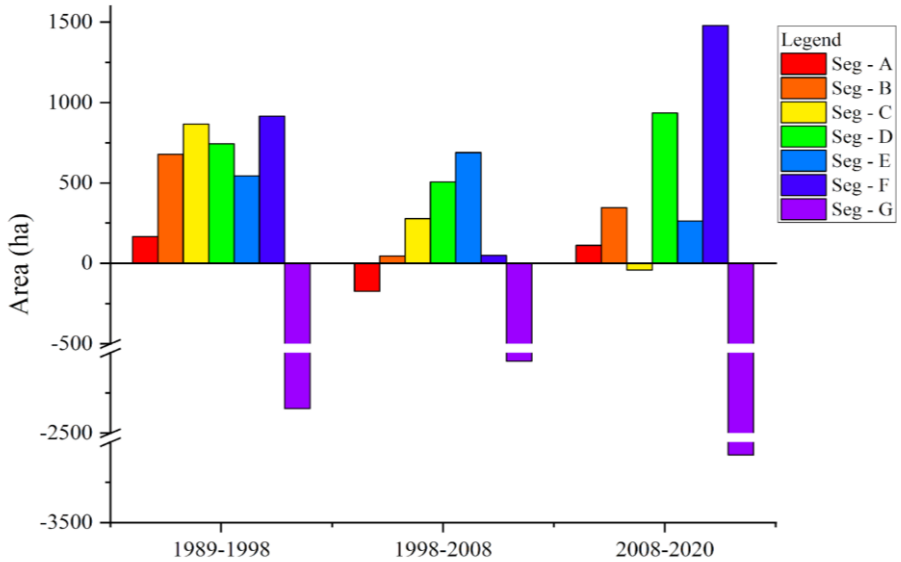

Figure 23. The balance chart for the accretion - erosion area in the study area

4.2. Shoreline changes affect and prevent solutions

Changing shorelines affect livelihoods in a variety of ways, especially coastal population activities.

Property damage and loss: shoreline change can result in losing or damaging homes, businesses, and other properties along the coast. This can cause significant financial and emotional distress for those affected.

Displacement: shoreline change can force people to move away from their homes and communities, either temporarily or permanently, due to the risk of flooding, erosion, or other hazards.

10.57647/j.ijes.2025.16851

Loss of livelihoods: coastal communities that rely on fishing, tourism, or other industries may experience a decline in their livelihoods due to the loss of beaches, wetlands, or other natural resources impacted by shoreline change.

Infrastructure damage: shoreline change can damage or destroy infrastructure such as roads, bridges, and other critical facilities. This can lead to disruptions in transportation, communication, and access to emergency services.

Integrated River Basin Management: Effective management of sediment discharge in the Mekong River requires a multifaceted approach that combines strong regulatory frameworks, community involvement, and innovative mitigation strategies. By prioritizing sustainability and cooperation. Governments and stakeholders consider the entire river basin, including upstream and downstream areas, to balance development with environmental sustainability. Policies should promote data sharing, joint monitoring, and coordinated management efforts. Encourage the design and operation of dams that minimize sediment trapping. Implement stricter regulations on sand mining, including licensing and monitoring of extraction activities, to ensure they are conducted sustainably. Prohibit sand mining in ecologically sensitive areas, particularly where it could exacerbate erosion or harm local livelihoods. The Mekong River Commission (MRC) is a typical example.

The coast of the Mekong Delta is made up mainly of clay and fine sand. Under the impact of waves, the coastal structure is easily broken. The majority of the shoreline material will transform into suspended sand after being broken due to the extremely tiny grain composition, which is easily carried by waves and coastal currents. The fact shows that the change in shoreline due to the processes of erosion and accretion is an unstable problem, often changing over time and space. Therefore, activities such as studying and monitoring changes in vegetation erosion and accretion in the Mekong Delta require a lot of time, effort, intelligence, and research technology. In particular, monitoring data also needs to be focused on, invested in, and cared for regularly to provide long-term and reliable data for research. It requires us to have hydrometeorological monitoring stations that monitor the amount of silt and transport sediment in both river and estuary areas. Simple erosion prevention techniques were once used, but they worked only temporarily. Before the force of the sea waves, they were quickly damaged and washed away.

The following remedies can be used to stop vegetation erosion and accretion's negative effects:

1. *Construction of a breakwater wall*: This is a rather expensive anti-erosion measure to prevent bank erosion and protect important works, cities, or valuable historical and cultural relics. It should be noted that the breakwater wall is only long-term effective when there is a solid foundation on which to build it.

2. *Breakwater dyke*: The purpose of a breakwater dyke is to stop bank retreat erosion gradation while also preventing salt water from entering the field. The breakwater anvil can be constructed out of reinforced concrete blocks or with stones, pebbles, gravel, or sand, with the grain size being increased from the dike body to the dyke roof on the seaward side. Because the roof of the breakwater is made of corrugated rock, which limits the height of the waves, it has an advantage over the breakwater wall in terms of cost and efficiency at absorbing wave energy. Furthermore, because the structure made of rocks, pebbles, gravel, and sand is soft, it does not require an extremely stable ground and is also simple to repair when it becomes deformed due to erosion.

3. *Welding torch* (welding torch dam): The welding torch is constructed perpendicularly or diagonally to the shoreline to divert waves, lessen wave energy, and simultaneously collect and accumulate sand, forming mud flats to prevent shoreline erosion or the process of accretion of creeks in seaports and estuaries. The soldering iron is often I- or T-shaped and can be floating or submerged.

Figure 24. a) Sandbags are used to temporarily prevent erosion when water overflows into residential areas; b) A section of the coast experienced serious erosion due to large waveshitting the dyke body on the coast of Tra Vinh province; c) A coastal erosion in Ben Tre province (February 2023) (Photo by the Bui Minh Quan)

10.57647/j.ijes.2025.16851

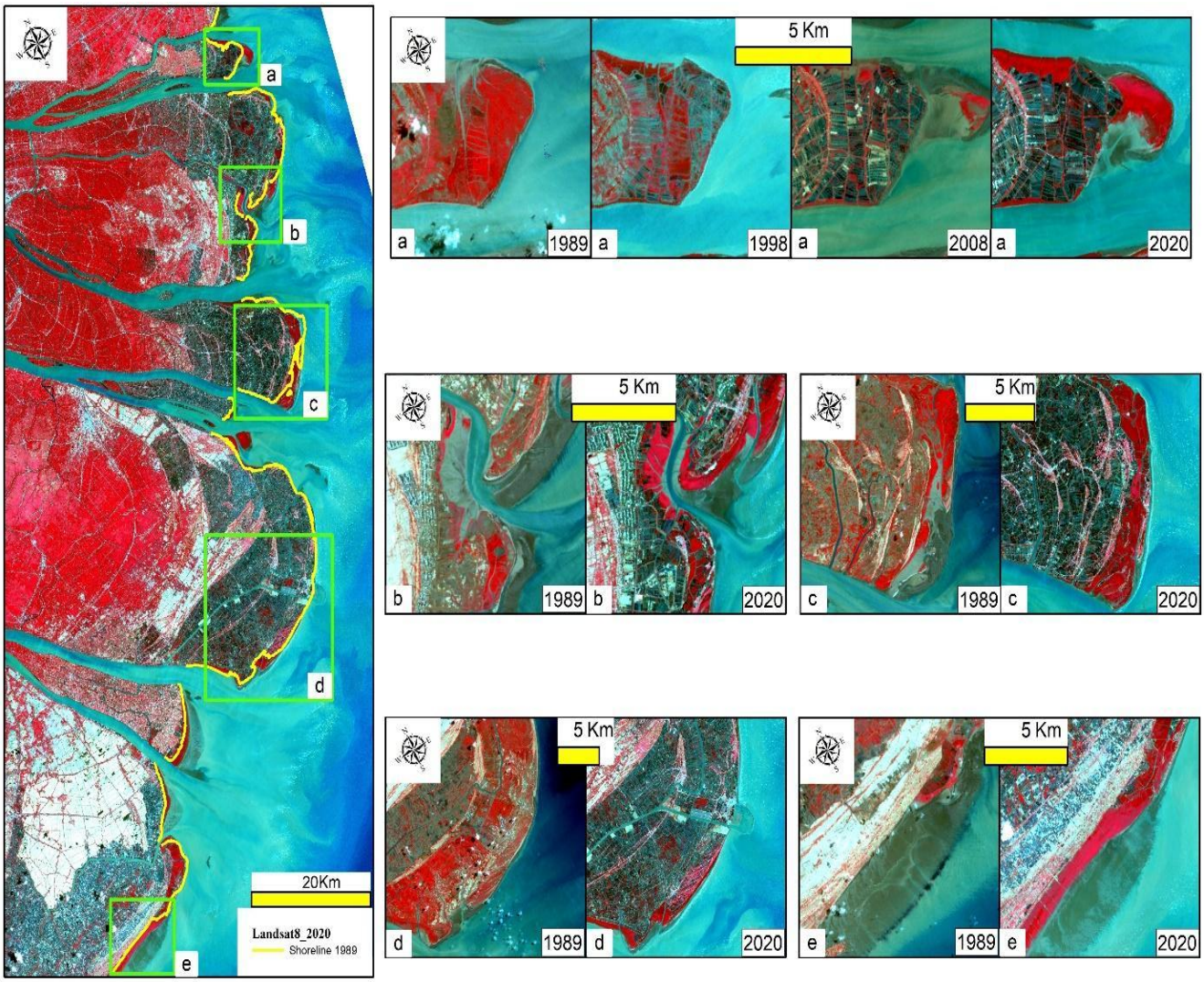

Figure 25. Geomorphological characteristics of the Mekong estuary. The shoreline displacement and evolution can be seen from satellite images over a certain period of time. The false color composites (NIR-Red-Green) with vegetation are shown in red

4. *Breakwater:* A structure built in the coastal sea that usually extends parallel to the coast. Breakwaters can be erected floating or submerged. In the event of high waves, breakwaters are frequently incorporated into the system. They are typically 50 to 200 meters long and 100 to 200 meters away from the beach. Breakwaters are constructed to stop waves from directly impacting the coast and to form sandbanks that prevent erosion beyond the breakwater.

5. *Diversion dams*: In estuaries with large sedimentation, measures to build diversion dams are implemented to prevent mud and sand from accumulating on both banks of the estuaries, to clear channels, and to prevent channel deformation. Dams are built to extend the length of the estuary from the shore to the sea.

None of the erosion mitigation strategies are everlasting; they all have a lifespan. The price of upkeep will keep rising during that period. When we interfere with accretion in one place, erosion will occur elsewhere because the total equilibrium will not change. Silent insufficiency is still the main factor and we can confirm that any measure to prevent erosion or accretion is only temporary support.

5. Conclusions

The Mekong Delta's coastal alterations were calculated using Landsat high-resolution satellite data combined with the Digital Shoreline Analysis System method (DSAS) and shoreline decomposition using the Normalized Difference Vegetation Index, the study effectively assessed shoreline vulnerability despite some uncertainties.

1. Between 1989 and 2020, the Mekong Delta shoreline was alternately eroded and accretion. Erosion and deposition occurred at different mouths and at different rates during the study period. Erosion and accretion rates in the Mekong River estuary by segment: The Tieu mouth to Dai mouth erosion and accretion are 82.42 m/yr and

10.57647/j.ijes.2025.16851

74.94 m/yr, respectively. In the Ba Lai mouth, erosion and accretion are 49.88 m/yr and 108.19 m/yr, respectively. In the Ham Luong mouth, erosion and accretion are 120.98 m/yr and 115.16 m/yr, respectively. The Co Chien mouth to Cung Hau mouth, erosion and accretion are 79.9 m/yr and 106.93 m/yr, respectively. The Dinh An mouth to Tran De mouth erosion and accretion are 1.37 m/yr and 117.06 m/yr, respectively.

2. The coast along the southern estuary from My Thanh to Ganh Hao estuary is primarily accretion (average: 7.69 m/yr), erosion and accretion are 66.07 m/yr and 91.06 m/yr, respectively. But the coast from Ganh Hao estuary to Ca Mau cape is erosion (average: 29.49 m/yr), erosion and accretion are 115.5 m/yr and 29.67 m/yr, respectively.

3. The cause of the decay is the lack of sediment due to the construction of hydroelectric dams in the upper Mekong River, large-scale sand mining every year, and the amount of sediment provided downstream cannot meet the demand enough, or land subsidence, as they create traps to catch the silt before it reaches the sea. Sea level rise: due to climate change, global sea levels are rising, threatening coastlines with increased saltwater intrusion and wave erosion. Coastal ecosystem degradation: as these ecosystems are degraded due to overfishing or climate change, coastlines become more vulnerable to waves and currents.

The study emphasizes the importance of developing Integrated Coastal Zone Management plans to address these changes and mitigate future risks. Current solutions to help the Mekong Delta resist erosion and accretion include planting coastal mangroves and constructing breakwaters and diversion dams. If we don't work together to protect the Mekong Delta's shoreline and the entire delta region in general, about 90% of the Mekong Delta will disappear by 2100. The insights gained from this research will guide future policy directions to protect and conserve the Mekong River Delta in the face of climate change.

Acknowledgements

This research is funded by the Ministry of Education and Training under grant number CT.2022.01.MDC.05.

Authors Contribution
All the authors have participated sufficiently in the intellectual content, conception, and design of this work or the analysis and interpretation of the data (when applicable), as well as the writing of the manuscript.

Availability of data and materials
The data that support the findings of this study are available from the corresponding author upon reasonable request.

Conflict of interest
The author states that there is no conflict of interest.

References

Anthony, E. J., Brunier, G., Besset, M., Goichot, M., Dussouillez, P., Nguyen, V. L. 2015. Linking rapid erosion of the Mekong River delta to human activities. *Scientific Reports*, 5, pp. 1–12. DOI: https://doi.org/10.1038/srep14745

Arjmandzadeh, R., Rashvanlou, V. S., Dabiri, R. and Almasi, A. 2017. Satellite thermal surveys to detecting hidden active faults and fault termination, case study of Quchan fault, NE Iran. *Iranian Journal of Earth Sciences*, 9(1), pp. 39–47.

Bao, T. Q. 2011. Effect of mangrove forest structures on wave attenuation in coastal Vietnam. *Oceanologia*, 53, pp. 807–818. DOI: https://doi.org/10.5697/oc.53-3.807

Bera, R. and Maiti, R. 2019. Quantitative analysis of erosion and accretion (1975–2017) using DSAS — a study on Indian Sundarbans. *Regional Studies in Marine Science*, 28, 100583. DOI: https://doi.org/10.1016/j.rsma.2019.100583

Besset, M., Brunier, G. and Anthony, E. 2015. Recent morphodynamic evolution of coastline of Mekong River Delta, towards an increased vulnerability. *Geophysical Research Abstracts*, 17, 2015–5427.

Besset, M., Anthony, E. J., Brunier, G. and Dussouillez, P. 2016. Shoreline change of the Mekong River delta along the southern part of the South China Sea coast using satellite image analysis (1973–2014). *Géomorphologie: relief, processus, environnement*, 22, pp. 137–146. DOI: https://doi.org/10.4000/geomorphologie.11336

Binh, D. V., Kanoush, S., Mai, N. P. and Sumi, T. 2018. Water level changes under increased regulated flows and degraded river in Vietnamese Mekong Delta. *Journal of Japan Society of Civil Engineers*, Ser. B1 (Hydraulic Engineering), 74, pp. 871–876. DOI: https://doi.org/10.2208/jscejhe.74.5_i_871

Boretti, A. 2020. Implications on food production of the changing water cycle in the Vietnamese Mekong Delta. *Global Ecology and Conservation*, 22, e00989. DOI: https://doi.org/10.1016/j.gecco.2020.e00989

Bravard, J., Goichot, M. and Gaillot, S. 2013. Geography of sand and gravel mining in the Lower Mekong River: first survey and impact assessment. *EchoGéo*, 26, pp. 1–18. DOI: https://doi.org/10.4000/echogeo.13659

Coleman, J. M. and Roberts, H. H. 1989. Deltaic coastal wetlands. *Coastal Lowlands, Geology and Geotechnology, Proceedings of the KNGMG Symposium, The Hague*, 24, pp. 1–24.

Commission Mekong River. 2005. Overview of the hydrology of the Mekong Basin. *Mekong River Commission*, report.

Dalrymple, R. W., Zaitlin, B. A. and Boyd, R. 1992. Estuarine facies models: conceptual basis an stratigraphic implications. *Journal of Sedimentary Petrology*, 62, pp. 1130–1146. DOI: https://doi.org/10.1306/D4267A69-2B26-11D7-8648000102C1865D

Dar, I. A. and Dar, M. A. 2009. Prediction of shoreline recession using geospatial technology: a case study of Chennai coast, Tamil Nadu, India. *Journal of Coastal Research*, 25, pp. 1276–1286. DOI: https://doi.org/10.2112/JCOASTRES-D-09-00051.1

Do, V. L. 2016. Final result report of investigation and assessment of modern geodynamics to improve climate change scenarios and adaptation solution proposals in Mekong Plain. *Geological Information Centre and Museum, Vietnam Geological Department*, 500 p. (in Vietnamese).

Fan, D., Nguyen, D. V., Su, J., Bui, V. V. and Tran, D. L. 2019. Coastal morphological changes in the Red River Delta under increasing natural and anthropic stresses. *Anthropocene Coasts*, 2, pp. 51–71.

DOI: https://doi.org/10.1139/anc-2018-0022

Fletcher, C. H., Romine, B. M., Genz, A. S., Barbee, M. M., Dyer, M., Anderson, T. R., Lim, S. C., Vitousek, S., Bochicchio, C. and Richmond, B. M. 2012. National assessment of shoreline change: historical shoreline change in the Hawaiian Islands. *U.S. Geological Survey Open-File Report 2011–1051*, 55 p.

Gebhardt, S., Nguyen, L. D. and Kuenzer, C. 2012. Mangrove ecosystems in the Mekong Delta – overcoming uncertainties in inventory mapping using satellite remote sensing data. *Springer Environmental Science and Engineering*, pp. 315–330.
DOI: https://doi.org/10.1007/978-94-007-3962-8_12

Griffin, M. and Burke, H. 2003. Compensation of hyperspectral data for atmospheric effects. *Lincoln Laboratory Journal*, 14, pp. 29–54.

Gugliotta, M., Saito, Y., Nguyen, V. L., Ta, T. K. O., Nakashima, R., Tamura, T., Uehara, K., Katsuki, K., Yamamoto, S. 2017. Process regime, salinity, morphological, and sedimentary trends along the fluvial to marine transition zone of the mixed-energy Mekong River delta, Vietnam. *Continental Shelf Research*, 147, pp. 7–26.
DOI: https://doi.org/10.1016/j.csr.2017.03.001

Ha, D. T., Ouillon, S. and Van, V. G. 2018. Water and suspended sediment budgets in the lower Mekong from high-frequency measurements (2009–2016). *Water (Switzerland)*, 10, 846.
DOI: https://doi.org/10.3390/w10070846

Jayson-Quashigah, P. N., Addo, K. A. and Kodzo, K. S. 2013. Medium resolution satellite imagery as a tool for monitoring shoreline change. Case study of the eastern coast of Ghana. *Journal of Coastal Research*, 65, pp. 511–516.
DOI: https://doi.org/10.2112/si65-087.1

Khoi, D. N., Dang, T. D., Pham, L. T. H., Loi, P. T., Thuy, N. T. D. and Phung, N. K., Bay, N. T. 2020. Morphological change assessment from intertidal to river-dominated zones using multiple-satellite imagery: a case study of the Vietnamese Mekong Delta. *Regional Studies in Marine Science*, 34, 101087.
DOI: https://doi.org/10.1016/j.rsma.2020.101087

Kondolf, G. M., Rubin, Z. K. and Minear, J. T. 2014. Dams on the Mekong: cumulative sediment starvation. *Water Resources Research*, 50, pp. 5158–5169.
DOI: https://doi.org/10.1002/2013WR014651

Kummu, M., Lu, X. X., Rasphone, A., Sarkkula, J. and Koponen, J. 2008. Riverbank changes along the Mekong River: remote sensing detection in the Vientiane-Nong Khai area. *Quaternary International*, 186, pp. 100–112.
DOI: https://doi.org/10.1016/j.quaint.2007.10.015

Li, X., Liu, J. P., Saito, Y. and Nguyen, V. L. 2017. Recent evolution of the Mekong Delta and the impacts of dams. *Earth-Science Reviews*, 175, pp. 1–17.
DOI: https://doi.org/10.1016/j.earscirev.2017.10.008

Li, Y., Chen, A., Mao, G., Chen, P., Huang, H., Yang, H., Wang, Z., Wang, K., Chen, H., Meng, Y., Zhong, R., Wang, P., Wang, H. and Liu, J. 2023. Multi-model analysis of historical runoff changes in the Lancang-Mekong River Basin – characteristics and uncertainties. *Journal of Hydrology*, 619, 129297.
DOI: https://doi.org/10.1016/j.jhydrol.2023.129297

Liu, J. P., Demaster, D. J., Nittrouer, C. A. and Eidam, E. F., Nguyen, T. T. 2017.A seismic study of the Mekong subaqueous delta: proximal versus distal sediment accumulation. *Continental Shelf Research*, 147, pp. 1–16.
DOI: https://doi.org/10.1016/j.csr.2017.07.009

Loisel, H., Mangin, A., Vantrepotte, V., Dessailly, D., Ngoc Dinh, D., Garnesson, P., Ouillon, S., Lefebvre, J. P., Mériaux, X. and Minh Phan, T. 2014. Variability of suspended particulate matter concentration in coastal waters under the Mekong's influence from ocean color (MERIS) remote sensing over the last decade. *Remote Sensing of Environment*, 150, pp. 218–230.
DOI: https://doi.org/10.1016/j.rse.2014.05.006

Lu, X. X. and Siew, R. Y. 2006. Water discharge and sediment flux changes over the past decades in the Lower Mekong River: possible impacts of the Chinese dams. *Hydrology and Earth System Sciences*, 10, pp. 181–195.
DOI: https://doi.org/10.5194/hess-10-181-2006

Marchesiello, P., Nguyen, N. M., Gratiot, N., Loisel, H., Anthony, E. J., Dinh, C. S., Nguyen, T., Almar, R. and Kestenare, E. 2019. Erosion of the coastal Mekong delta: assessing natural against man induced processes. *Continental Shelf Research*, 181, pp. 72–89.
DOI: https://doi.org/10.1016/j.csr.2019.05.004

Meade, R. H. 1996.River-sediment inputs to major deltas. In Sea-Level Rise and Coastal Subsidence: Causes, Consequences and Strategies. *Coastal Systems and Continental Margins*, 2, pp. 63–85.
DOI: https://doi.org/10.1007/978-94-015-8719-8_4

Milliman, J. D. and Syvitski, J. P. M. 1992. Geomorphic/tectonic control of sediment discharge to the ocean: the importance of small mountainous rivers. *Journal of Geology*, 100, pp. 525–544.
DOI: https://doi.org/10.1086/629606

Milliman, J. D. and Farnsworth, K. L. 2011. River discharge to the coastal ocean: a global synthesis. *Cambridge University Press*, 384 p.
DOI: https://doi.org/10.1017/CBO9780511781247

Minderhoud, P. S. J., Erkens, G., Pham, V. H., Bui, V. T., Erban, L., Kooi, H. and Stouthamer, E. 2017. Impacts of 25 years of groundwater extraction on subsidence in the Mekong Delta, Vietnam. *Environmental Research Letters*, 12, 064006.
DOI: https://doi.org/10.1088/1748-9326/aa7146

MRC. 2005. Overview of the hydrology of the Mekong Basin. Mekong River Commission, report.

Nguyen, A. D. and Savenije, H. H. G. 2006. Salt intrusion in multi-channel estuaries: a case study in the Mekong Delta, Vietnam. *Hydrology and Earth System Sciences*, 10, pp. 743–754.
DOI: https://doi.org/10.5194/hess-10-743-2006

Nowacki, D. J., Ogston, A. S., Nittrouer, C. A., Fricke, A. T. and Pham, D. T., Van 2015. Sediment dynamics in the lower Mekong River: transition from tidal river to estuary. *Journal of Geophysical Research*: Oceans, 120, pp. 6363–6383.
DOI: https://doi.org/10.1002/2015JC010754

Pawar, U., Try, S., Muttil, N., Rathnayake, U. and Suppawimut, W. 2023. Frequency and trend analyses of annual peak discharges in the Lower Mekong Basin. *Heliyon*, 9, e19690.
DOI: https://doi.org/10.1016/j.heliyon.2023.e19690

Phan, H. M., Reniers, A., Ye, Q. and Stive, M. 2017. Response in the Mekong deltaic coast to its changing sediment sources and sinks. *Proceedings of Coastal Dynamics 2017*, pp. 311–322.
Repository: http://repository.tudelft.nl/record/uuid:e964293a-f6e9-4ae1-ba51-a550e9ad3cc0

Phan, L. K., Van Thiel De Vries, J. S. M. and Stive, M. J. F. 2015. Coastal mangrove squeeze in the Mekong Delta. *Journal of Coastal Research*, 31, pp. 233–243.
DOI: https://doi.org/10.2112/JCOASTRES-D-14-00049.1

Rouse, J. W., Haas, R. H., Schell, J. A. and Deeering, D. 1973. Monitoring vegetation systems in the Great Plains with ERTS (Earth Resources Technology Satellite). *Third Earth Resources Technology Satellite-1 Symposium, 1*, pp. 309–317.

Smajgl, A., Toan, T. Q., Nhan, D. K., Ward, J., Trung, N. H., Tri, L. Q., Tri, V. P. D. and Vu, P. T. 2015. Responding to rising sea levels in the Mekong Delta. *Nature Climate Change*, 5, pp. 167–174.
DOI: https://doi.org/10.1038/nclimate2469

Souza Filho, P. W. M., Farias Martins, E. do S. and da Costa, F. R. 2006. Using mangroves as a geological indicator of coastal changes in the Bragança macrotidal flat, Brazilian Amazon: a remote sensing data approach. *Ocean and Coastal Management*, 49, pp. 462–475. DOI: https://doi.org/10.1016/j.ocecoaman.2006.04.005

Syvitski, J. P. M., Charles, J. V., Albert, J. K. and Pamela, G. 2005. Impact of humans on the flux of terrestrial sediment to the global coastal ocean. *Science (New York, N.Y.)*, 308, pp. 376–380. DOI: https://doi.org/10.1126/SCIENCE.1109454

Ta, T. K. O., Nguyen, V. L., Tateishi, M., Kobayashi, I., Saito, Y., Nakamura, T. 2002. Sediment facies and Late Holocene progradation of the Mekong River Delta in Bentre Province, southern Vietnam: An example of evolution from a tide-dominated to a tide- and wave-dominated delta. *Sedimentary Geology*, 152, pp. 313–325. DOI: https://doi.org/10.1016/S0037-0738(02)00098-2

Ta, T. K. O., Nguyen, V. L., Tateishi, M., Kobayashi, I., Saito, Y. 2005. Holocene Delta Evolution and Depositional Models of the Mekong River Delta, Southern Vietnam. *River Deltas-Concepts, Model, and Examples*, pp. 453–466. DOI: https://doi.org/10.2110/pec.05.83.0453

Tamura, T., Horaguchi, K., Saito, Y., Nguyen, V. L., Tateishi, M., Ta, T. K. O., Nanayama, F., Watanabe, K. 2010. Monsoon-influenced variations in morphology and sediment of a mesotidal beach on the Mekong River delta coast. *Geomorphology*, 116, pp. 11–23. DOI: https://doi.org/10.1016/j.geomorph.2009.10.003

Thieler, E. R., Himmelstoss, E. A., Zichichi, J. L., Ergul, A. 2009. The Digital Shoreline Analysis System (DSAS) Version 4.0 - An ArcGIS extension for calculating shoreline change. *Open-File Report*. DOI: https://doi.org/10.3133/OFR20081278

Tong, P. H. S., Auda, Y., Populus, J., Aizpuru, M., Al Habshi, A., Blasco, F. 2004. Assessment from space of mangroves evolution in the Mekong Delta, in relation to extensive shrimp farming. *International Journal of Remote Sensing*, 25, pp. 4795–4812. DOI: https://doi.org/10.1080/01431160412331270858

Unverricht, D., Szczuciński, W., Stattegger, K., Jagodziński, R., Le, X. T., Kwong, L. L. W. 2013. Modern sedimentation and morphology of the subaqueous Mekong Delta, Southern Vietnam. *Global and Planetary Change*, 110, pp. 223–235. DOI: https://doi.org/10.1016/j.gloplacha.2012.12.009

Unverricht, D., Nguyen, T. C., Heinrich, C., Szczuciński, W., Lahajnar, N., Stattegger, K. 2014. Suspended sediment dynamics during the inter-monsoon season in the subaqueous Mekong Delta and adjacent shelf, southern Vietnam. *Journal of Asian Earth Sciences*, 79, pp. 509–519. DOI: https://doi.org/10.1016/j.jseaes.2012.10.008

Vörösmarty, C. J., Meybeck, M., Fekete, B., Sharma, K., Green, P., Syvitski, J. P. M. 2003. Anthropogenic sediment retention: Major global impact from registered river impoundments. *Global and Planetary Change*, 39, pp. 169–190. DOI: https://doi.org/10.1016/S0921-8181(03)00023-7

Vu, M. T., Lacroix, Y., Than, V. V., Nguyen, V. T. 2020. Prediction of shoreline changes in Almanarre beach using geospatial techniques. *Indian Journal of Geo-Marine Sciences*, 49, pp. 207–217.

Wang, J. J., Lu, X. X., Kummu, M. 2011. Sediment load estimates and variations in the lower Mekong River. *River Research and Applications*, 27, pp. 33–46. DOI: https://doi.org/10.1002/rra.1337

Yazdi, A., ShahHoseini, E., Razavi, R. 2016. AMS, A method for determining magma flow in Dykes (Case study: Andesite Dyke). *Research Journal of Applied Sciences*, 11(3), pp. 62–67. DOI: http://doi.org/10.3923/rjasci.2016.62.67